

10-11-2024

Genetic Knock-In of EIF2AK3 Variants Reveals Differences in PERK Activity in Mouse Liver and Pancreas Under Endoplasmic Reticulum Stress

Shivesh Ghura

Noah R. Beratan


Xinglong Shi

Elena Alvarez-Periel

Sarah E. Bond Newton

See next page for additional authors

Follow this and additional works at: <https://jdc.jefferson.edu/farberneurospapers>

 Part of the [Medical Genetics Commons](#), and the [Translational Medical Research Commons](#)

[Let us know how access to this document benefits you](#)

This Article is brought to you for free and open access by the Jefferson Digital Commons. The Jefferson Digital Commons is a service of Thomas Jefferson University's [Center for Teaching and Learning \(CTL\)](#). The Commons is a showcase for Jefferson books and journals, peer-reviewed scholarly publications, unique historical collections from the University archives, and teaching tools. The Jefferson Digital Commons allows researchers and interested readers anywhere in the world to learn about and keep up to date with Jefferson scholarship. This article has been accepted for inclusion in Farber Institute for Neuroscience Staff Papers and Presentations by an authorized administrator of the Jefferson Digital Commons. For more information, please contact: JeffersonDigitalCommons@jefferson.edu.

Authors

Shivesh Ghura, Noah R. Beratan, Xinglong Shi, Elena Alvarez-Periel, Sarah E. Bond Newton, Cagla Akay-Espinoza, and Kelly L. Jordan-Sciutto



OPEN Genetic knock-in of *EIF2AK3* variants reveals differences in PERK activity in mouse liver and pancreas under endoplasmic reticulum stress

Shivesh Ghura¹, Noah R. Beratan¹, Xinglong Shi¹, Elena Alvarez-Periel¹, Sarah E. Bond Newton^{1,2}, Cagla Akay-Espinoza¹ & Kelly L. Jordan-Sciutto¹✉

Common single-nucleotide variants (SNVs) of eukaryotic translation initiation factor 2 alpha kinase 3 (*EIF2AK3*) slightly increase the risk of disorders in the periphery and the central nervous system. *EIF2AK3* encodes protein kinase RNA-like endoplasmic reticulum kinase (PERK), a key regulator of ER stress. Three exonic *EIF2AK3* SNVs form the PERK-B haplotype, which is present in 28% of the global population. Importantly, the precise impact of these SNVs on PERK activity remains elusive. In this study, we demonstrate that PERK-B SNVs do not alter PERK expression or basal activity in vitro and in the novel triple knock-in mice expressing the exonic PERK-B SNVs in vivo. However, the kinase activity of PERK-B protein is higher than that of PERK-A in a cell-free assay and in mouse liver homogenates. Pancreatic tissue in PERK-B/B mice also exhibit increased susceptibility to apoptosis under acute ER stress. Monocyte-derived macrophages from PERK-B/B mice exhibit higher PERK activity than those from PERK-A/A mice, albeit with minimal functional consequences at acute timepoints. The subtle PERK-B-driven effects observed in liver and pancreas during acute stress implicate PERK as a contributor to disease susceptibility. The novel PERK-B mouse model provides valuable insights into ER stress-induced PERK activity, aiding the understanding of the genetic basis of disorders associated with ER stress.

Keywords Endoplasmic reticulum, Stress, Unfolded protein response, *EIF2AK3*, Single-nucleotide variant, Protein kinase RNA-like ER kinase, Haplotype

Genome-wide association studies (GWAS) play a pivotal role in advancing our understanding of polymorphic genes that influence disease risk. Nevertheless, there remains a debate on whether disease risk arises primarily from the cumulative impact of numerous common variants with minor effect sizes or from a limited number of rare variants with substantial effect sizes. The complex interplay of common variants and rare mutations is further complicated by intricate gene-gene, gene-environment, and epigenetic interactions that collectively shape the landscape of complex traits and disease susceptibility^{1–3}.

One emerging example of this complexity is eukaryotic translation initiation factor 2 alpha kinase 3 (*EIF2AK3*), which not only plays a role in signaling cascades involved in multiple physiologic and pathologic processes but also has an ascribed role as a causative or contributing factor in a range of pathologies. *EIF2AK3* encodes a kinase termed protein kinase RNA-like endoplasmic reticulum kinase (PERK), which is pivotal as an endoplasmic reticulum (ER) stress sensor in determining whether the cell should initiate an adaptive or apoptotic response. ER stress, which occurs in the setting of imbalance between the demand for protein synthesis and the ER folding capacity, can be aggravated by various endogenous and exogenous factors, including accumulation of unfolded/misfolded proteins, release of ER Ca²⁺, viral infection, hypoxia, and anemia. In response to these stressors, cells activate the unfolded protein response (UPR), a multifaceted and overlapping set of pathways to restore cellular homeostasis during stress or, alternatively, drive the cell toward apoptosis^{4,5}. PERK exerts its effects by phosphorylating its primary substrate, eukaryotic initiation factor 2α (eIF2α), which halts global translation, allowing the cell to resolve ER stress. However, certain proteins harboring multiple upstream open reading frames can evade translational pause; the mRNA encoding activating transcription factor 4 (ATF4) is one such

¹Department of Oral Medicine, School of Dental Medicine, University of Pennsylvania, 240 S. 40th St, Rm 312 Levy, Philadelphia, PA 19104, USA. ²Department of Neuroscience, Weinberg ALS Center, Farber Institute for Neuroscience, Thomas Jefferson University, Philadelphia, PA 19107, USA. ✉email: jordanak@upenn.edu

example^{6–9}. ATF4 upregulates distinct genes and transcription factors such as binding immunoglobulin protein (BIP) and the proapoptotic C/EBP homologous protein (CHOP) in a time- and stress-dependent manner^{10,11}. Other pathways involved downstream from PERK signaling through transcriptional regulation are endogenous antioxidant response, autophagy, and lipogenic pathways, among others^{12–15}.

A rare variant of *EIF2AK3* is associated with high risk for Wolcott-Rallison syndrome (WRS), which arises from mutations within or near the catalytic kinase domain of PERK and manifests as permanent neonatal or early infancy insulin-dependent diabetes, liver dysfunction, growth retardation, osteoporosis, and cognitive deficits^{16,17}. Conversely, common single-nucleotide variants (SNVs) of *EIF2AK3* have been reported to be associated with mild to moderate risk for several diseases in the periphery and the central nervous system (CNS)^{16,18–24}. Specifically, the minor alleles of three nonsynonymous *EIF2AK3* SNVs (rs867529, rs13045, and rs1805165) were associated with increased risk of progressive supranuclear palsy (PSP)^{21,22} and growth hormone deficiency²³ whereas one study reported their association with late-onset Alzheimer's disease (AD) in individuals carrying the *APOE ε4* allele, the greatest genetic risk factor for AD²⁴. Furthermore, we recently reported that the minor alleles of these three SNVs were associated with increased risk of neurocognitive impairment, increased cerebrospinal fluid levels of interleukin 6, and increased frequency of depressive mood in people with HIV on antiretroviral therapy^{19,25}. The minor allele of rs867529 was also associated with higher risk of prediabetes and lung cancer in Chinese cohorts^{18,20}. Variation in *EIF2AK3* exhibits a range of risk for disorders associated with liver, pancreas and the CNS; however, models to examine the contribution of these variations to organ dysfunction are needed.

The major and minor alleles of rs867529, rs13045, and rs1805165, form PERK-A and PERK-B, respectively, the two most common haplotypes of PERK, whereas the minor allele of rs13045 alone forms the much rarer PERK-D^{21,22,26}. The LD between rs867529 and rs1805165 is > 0.95 , whereas the r^2 is 0.73–0.74 between rs13045 and the other two SNVs. PERK-B is prevalent in approximately 28% of the global population in contrast to the more prevalent PERK-A haplotype, which is present in 64% of the population (<https://www.ncbi.nlm.nih.gov/clinvar>; accessed March 19, 2024). Importantly, these three SNVs have potential functional impact on PERK's kinase activity as they change two amino acids in the luminal domain (S136C [rs867529], R166Q [rs13045]) and one amino acid in the kinase domain (S704A [rs1805165]). However, conflicting evidence hinders the understanding of the impact of these SNVs on PERK regulation and activity^{27–29}. While lymphoblastoid cell lines derived from PERK-B-expressing individuals showed similar baseline PERK protein levels and exhibited higher PERK kinase activity, determined by p-eIF2 α levels following challenge with tunicamycin, which blocks N-linked glycosylation. In contrast, another study proposed PERK-B as a hypomorph with partial reduction in function, based on higher p-eIF2 α levels in PERK-A- as opposed to PERK-B-expressing cells, both at baseline and following treatment with thapsigargin, which inhibits the sarco-ER calcium ATPase pump to trigger ER stress³⁰.

We hypothesized that the PERK-B SNVs would exhibit increased PERK activity both in vitro and in vivo, particularly under acute ER stress conditions. We anticipated that the subtle changes induced by these SNVs, despite their relatively high frequency and moderate effect size in human studies, would not lead to significant outcomes in physiologic stressors such as aging and that their impact would likely be noticeable in artificial and exogenous acute stress conditions. To this end, we aimed to evaluate the risk of organ dysfunction associated with PERK-B SNVs in a novel knock-in mouse line, in which the amino acids of the PERK-B SNVs were introduced into *Eif2ak3* using CRISPR.

Results

PERK-B has higher kinase activity than PERK-A in a cell-free kinase assay

The conflicting results regarding the effects of PERK-B SNVs on PERK kinase activity^{27–29} suggest that the PERK kinase activity and regulation might be dependent on the cellular context. Thus, we first compared the kinase activities of PERK-A and PERK-B in a cell-free kinase assay to mitigate potential cell-specific influences. The comparison of the levels of recombinant eIF2 α phosphorylated by purified recombinant PERK-A and PERK-B revealed that the PERK-B kinase activity was significantly higher than that of PERK-A at both 30 and 60 min (Fig. 1, Supplementary Fig S1).

Baseline characteristics are similar between the novel triple knock-in PERK-B/B mice and the wild-type PERK-A/A mice

Previous studies have associated PERK-B SNVs to altered kinase activity and stress response^{27–29}, potentially elevating the risk of diseases affecting both the periphery and the CNS^{18–25}. To explore the potential impact of PERK-B SNVs on stress response within the cellular environment as well as within the context of an organism, we established a novel triple knock-in PERK-B mouse model. We sequentially introduced mutations in serine 132 (rs867529), arginine 162 (rs13045), and serine 700 (rs1805165) in wild-type mice (PERK-A/A) to generate PERK-B/B mice with cysteine 132, glutamine 162, and alanine 700 (Fig. 2a). Of note, these residues are conserved in the mouse.

First, we assessed the potential baseline alterations in PERK levels and downstream signaling partners, particularly focusing on the PERK/eIF2 α /ATF4 axis^{10,11}. The analysis of the tissue samples from the pancreas, liver, and brain of age- and sex-matched homozygous PERK-A/A and PERK-B/B mice revealed that PERK expression, its kinase activity, and downstream signaling components did not differ between the PERK-A/A and PERK-B/B mice at baseline (Fig. 2b–g, Supplementary Fig S2). We closely monitored allelic frequencies to ensure that the PERK-B SNVs followed Mendelian genetics (Supplementary Fig S3a). Additionally, we found no noticeable changes in mouse breeding or growth characteristics, including litter size, sex ratio, and age-related weight changes, between the PERK-B/B and PERK-A/A mice (Supplementary Fig S3b–e).

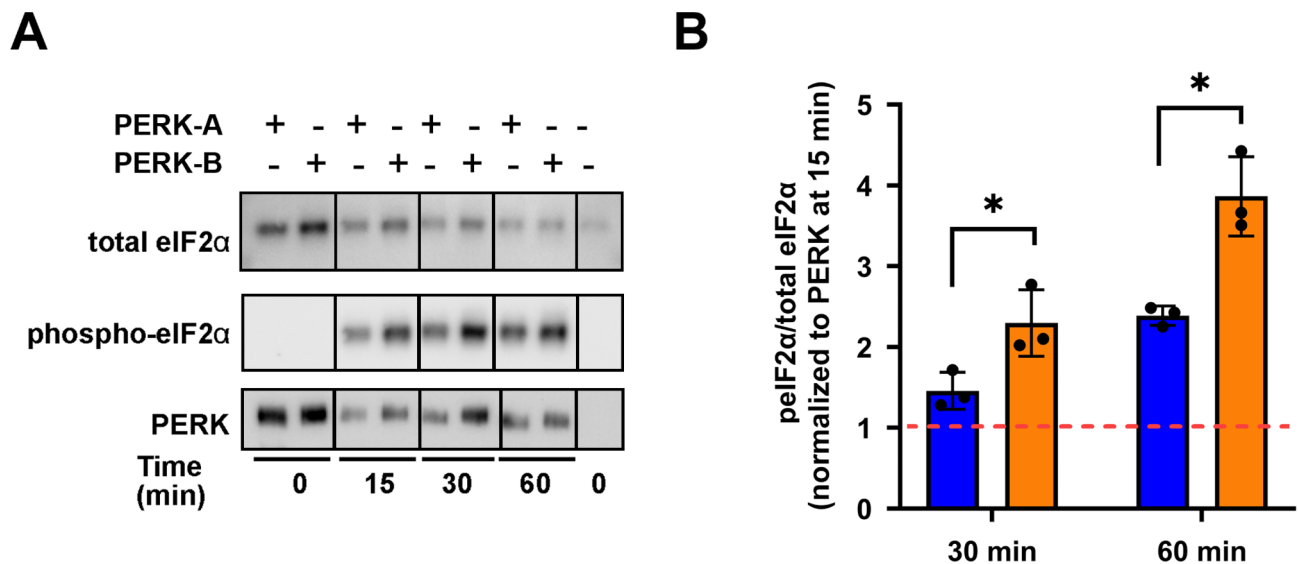


Fig. 1. PERK-B has higher kinase activity than PERK-A in a cell-free assay. **A.** Representative blots of the kinase assay, in which flag-tagged full-length PERK-A or PERK-B were incubated with recombinant eIF2α and ATP for 0–60 min ($n = 3$) and analyzed by immunoblotting with antibodies to phospho-eIF2α, total eIF2α, and PERK. **B.** Quantification of the cell-free PERK kinase assay, with normalization of the phospho-eIF2α/total eIF2α ratio to the corresponding PERK level. Red dashes indicate kinase activity at 15 min. * $p < 0.05$, two-way repeated measures analysis of variance (ANOVA) with Sidak's test for multiple comparisons.

Comparative pathologic analysis of young and old PERK-A/A, A/B, and B/B mice

Although we found no discernible differences in PERK expression levels and activity across the pancreas, liver, and brain between the PERK-A/A and PERK-B/B mice at baseline, we considered the potential age-related pathologies associated with PERK-B/B SNVs. To this end, we used a comprehensive panel of organ-specific histopathologic analyses in young (2–3 months) and old (13–14 months) cohorts of PERK-A/A, PERK-A/B, and PERK-B/B mice. We found no significant differences in any of the outcomes based on age, sex, or genotype (Fig. 3a–b). However, we noted subtle differences in the rates of lymphoid hyperplasia, protozoal outgrowth in the colon, acidophilic macrophage pneumonia, and eosinophilic crystalline pneumonia among the genotypes (Supplementary Fig S4a–c).

ER-stress-induced PERK activity is higher in PERK-B/B-expressing MDMs than in PERK-A/A-expressing MDMs in vitro

The conflicting data on the impact of PERK-B SNVs on PERK kinase activity reported in in vitro studies^{27–29} might be partially due to the cell-type-specific regulation. Recent studies underscore the pivotal role of PERK-mediated stress responses in macrophages during immune homeostasis^{31–34}. Based on our observation of a trend in the alteration of the phenotype of alveolar macrophages in old PERK-A/B mice compared to the age-matched PERK-A/A and PERK-B/B mice (Supplementary Fig S4a), we examined PERK activity in monocyte-derived macrophages (MDMs) generated from PERK-A/A and PERK-B/B mice. Consistent with our cell-free kinase assay, PERK kinase activity was higher in PERK-B/B MDMs than in PERK-A/A MDMs following thapsigargin treatment (Fig. 4a–b, Supplementary Fig S5). Of note, the MDMs in cultures expressed the myeloid markers F4/80 and CD11b, indicating effective differentiation (Supplementary Fig S6a–c).

Increased PERK activity in PERK-B/B MDMs is not associated with altered function in vitro

Given that PERK-B/B MDMs displayed higher PERK activity than PERK-A/A MDMs, we investigated three functional consequences of such differential activity: phagocytosis, viability in response to ER stress, and M1 versus M2-like phenotypes. In assessment of the phagocytic function by incubating the MDMs with opsonin-coated Cy3-labeled zymosan beads, we observed that the phagocytotic activity reached saturation at 40 min (Supplementary Fig S6c). Importantly, the phagocytosis efficiency was similar between the PERK-A/A and PERK-B/B MDMs, indicating that the PERK-B/B SNVs did not alter phagocytosis at baseline (Fig. 5a–b). Next, we examined cell survival following ER stress by treating PERK-A/A and PERK-B/B MDMs with varying doses of the ER stressors thapsigargin, tunicamycin, and the PERK activator CCT020312. We observed a significant reduction in viability with the higher dose of thapsigargin and CCT020312 as well as both the low and high doses of tunicamycin, with reduced cell survival comparable between the PERK-A/A and PERK-B/B MDMs (Fig. 5c–d).

Based on conflicting findings regarding the role of PERK in specific phenotypes of macrophages^{32,33,35}, we determined the impact of thapsigargin, tunicamycin, and the PERK activator on the RNA expression levels of proinflammatory (*Cd86* and *Cd80*) and anti-inflammatory (*Arg1* and *Cd206*) markers in PERK-A/A and PERK-B/B MDMs. As shown in Fig. 5e–h, while the *Cd86* expression levels were increased with high-dose thapsigargin

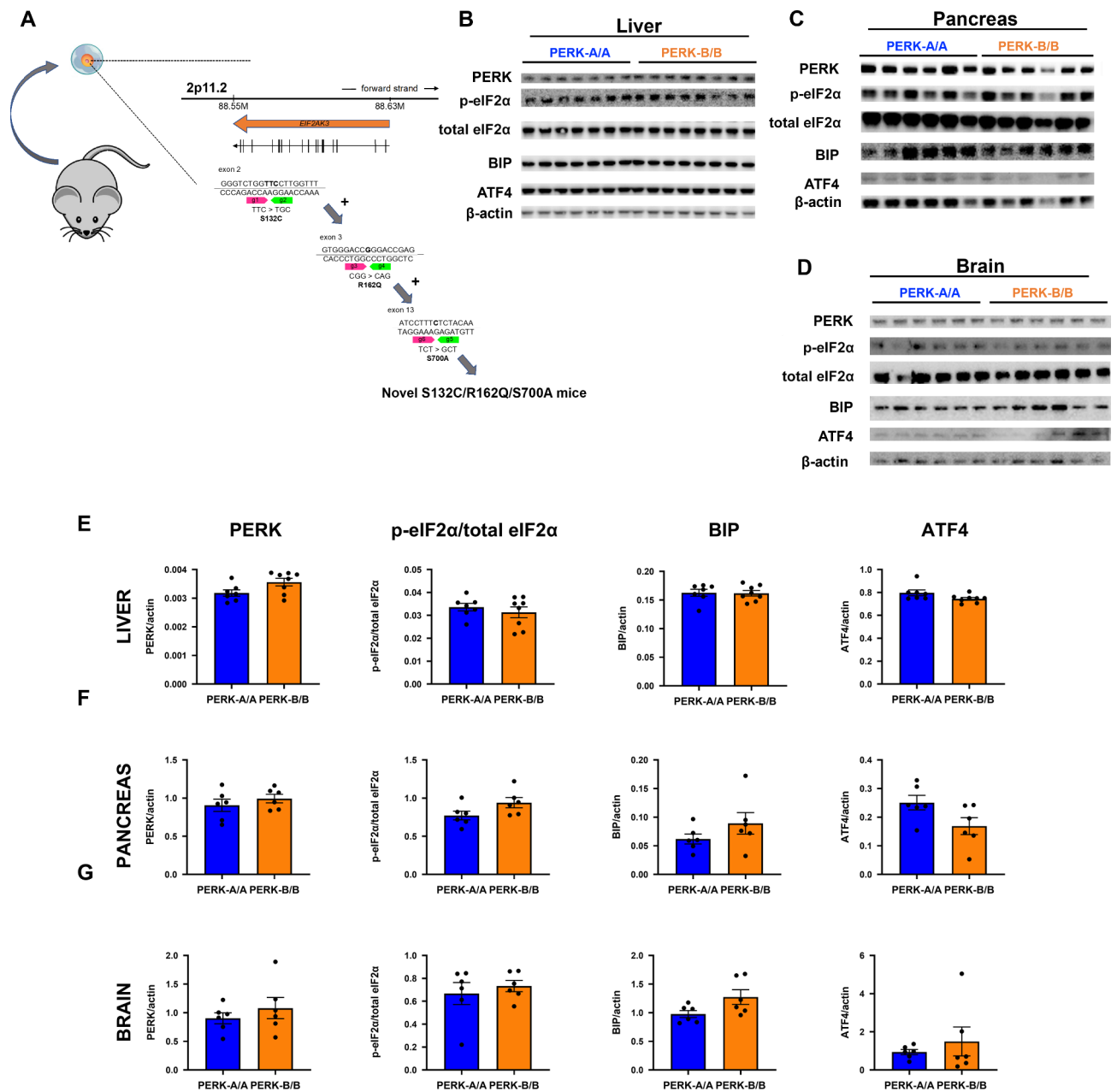


Fig. 2. Novel triple knock-in PERK-B/B mice express the three exonic single-nucleotide variants associated with PERK haplotype B. **A.** The three PERK-B exonic SNVs were introduced in the C57BL/6 mouse line by sequential mutation using CRISPR/Cas9, as illustrated. **B–D.** Tissue homogenates from the liver (**B**), pancreas (**C**), and brain (**D**) of 3-month-old PERK-A and PERK-B mice ($n = 3/\text{group}$) were analyzed for PERK protein expression and signaling downstream of PERK by immunoblotting. Representative blots are shown. **E–G.** Quantification of the immunoblots shows comparable protein levels of PERK, BIP, ATF4, and p-eIF2α at baseline in the liver (**E**), pancreas (**F**), and brain (**G**) between PERK-A/A and PERK-B/B mice. * $p < 0.05$, unpaired t test.

and tunicamycin, with a similar effect observed in both the PERK-A/A and PERK-B/B MDMs, the *Cd80*, *Arg1*, and *Cd206* expression levels did not exhibit notable changes in response to any of the three ER stressors at either dose or genotype (Fig. 5e–h).

Stress-induced PERK activity in liver is genotype-dependent

Disorders associated with *EIF2AK3* mutations, such as WRS, often result in dysfunction of the pancreas and liver^{16,36–38}. Therefore, although the PERK-B SNVs did not alter PERK expression or activity in the liver and pancreas at baseline, we next evaluated the potential differences in PERK kinase activity in the presence of ER stress. We examined the liver and pancreas of PERK-A/A and PERK-B/B mice 24 h after the intraperitoneal administration of tunicamycin (0.5 mg/kg). Tunicamycin treatment resulted in an increase in eIF2α

A

Lesion	PERK-A/A										PERK-A/B										PERK-B/B										Severity of change														
	Females					Males					Females					Males					Females					Males																			
	2045	2046	2047	2075	2076	2077	2048	2049	2050	2051	2073	2074	2075	2082	2068	2069	2071	2072	2082	2061	2062	2063	2064	2066	2081	2084	2085	2086	2052	2053			2054	2055	2083	2056	2057	2058	2059	2060					
Liver - inflammatory portal infiltrates	1	1	1	1	1	1	1	1	1	1	1	1	1	1	1	1	1	1	1	2	1	1	1	2	1	1	1	2	1	1	1	1	1	1	1	1	1	1	Unremark	0					
Liver - hepatocyte death	1	1	1	1	1	1	0	0	1	1	1	1	1	1	1	1	1	1	0	2	0	0	0	2	0	1	1	2	1	1	1	1	0	0	1	1	1	1	Minimal	1					
Liver - hepatocyte swelling and clearing	2	2	2	2	2	2	1	1	1	1	1	1	1	1	1	1	1	1	1	2	2	2	2	2	2	2	2	2	2	2	2	2	2	2	2	2	2	2	Mild	2					
Liver - extramedullary hematopoiesis	1	0	0	0	0	0	1	0	0	0	0	0	0	1	0	0	0	0	1	0	0	0	0	0	0	0	0	0	0	0	0	0	0	0	0	0	0	0	Moderate	3					
Liver - hepatic lipidosis	0	0	0	0	0	0	0	0	0	0	0	0	0	0	0	0	0	0	0	0	0	0	0	0	0	0	0	0	0	0	0	0	0	0	0	0	0	0	Severe	4					
Liver - hepatocellular neoplasm	0	0	0	0	0	0	0	0	0	0	0	0	0	0	0	0	0	0	0	0	0	0	0	0	0	0	0	0	0	0	0	0	0	0	0	0	0	0							
Liver - oval cell hyperplasia	0	0	0	0	0	0	0	0	0	0	0	0	0	0	0	0	0	0	0	0	0	0	0	0	0	0	0	0	0	0	0	0	0	0	0	0	0	2	0						
Liver - increased arteriolar profiles	0	0	0	0	0	0	0	0	0	0	0	0	0	0	0	0	0	0	0	0	0	0	0	0	0	2	0	0	0	0	0	0	0	0	0	0	0	0	2	0					
Gallbladder - inflammation	NA	NA	NA	NA	2	0	NA	2	0	0	0	0	0	2	NA	0	0	0	0	NA	0	0	0	0	0	0	NA	NA	0	0	0	0	NA	0	NA	0	2	NA	2	0					
Gallbladder - acidophilic droplets	NA	NA	0	NA	0	0	NA	0	0	0	0	0	0	0	0	0	0	0	NA	0	0	0	0	0	0	0	NA	NA	0	0	0	0	0	0	0	0	0	0	0	0					
Pancreas - inflammatory infiltrates	0	0	1	0	0	0	1	0	0	0	0	0	0	0	0	0	0	0	0	0	0	0	0	0	0	2	0	0	0	0	0	1	0	0	0	0	0	0	0	0					
Pancreas - vacuoles	0	0	2	0	0	0	0	0	0	0	0	0	0	0	0	0	0	0	0	0	0	0	0	0	0	0	0	0	0	0	0	0	0	0	0	0	0	2	0	0					
Pancreas - zymogen granule depletion	0	0	0	0	0	0	0	0	0	0	0	0	0	0	0	0	0	0	0	0	0	0	0	0	0	0	0	3	0	0	0	0	0	0	0	0	0	0	0	0					
Pancreas - atrophy	0	0	2	0	0	0	0	0	0	0	0	0	0	0	0	0	0	0	0	0	0	0	0	0	0	0	0	0	0	0	0	0	0	0	0	0	0	0	0	0					
Kidney - inflammatory infiltrates	0	0	1	0	0	1	0	0	0	1	0	0	0	1	0	0	0	0	0	0	0	0	0	0	0	0	1	0	0	0	1	2	1	1	1	2	1	0	0	0					
Kidney - tubular basophilia	1	0	0	1	1	0	0	0	0	0	0	0	0	0	0	0	0	0	0	0	0	0	0	0	0	0	0	1	1	0	0	0	0	0	0	0	0	0	0	0	0				
Lungs - inflammatory aggregates	1	0	0	1	1	0	0	0	0	1	0	1	0	2	1	0	1	2	1	1	0	0	0	0	0	0	0	1	1	1	0	0	0	0	0	0	0	0	0	0	0	0			
Lungs - acidophilic macrophages	0	0	0	0	0	0	0	0	0	0	0	0	0	0	0	0	0	0	0	0	0	0	0	0	0	2	0	0	0	0	0	0	0	0	0	0	0	0	0	0	0	0			
Lungs - alveolar histiocytosis	0	0	0	0	0	0	0	0	0	0	0	0	0	0	0	0	0	0	0	0	0	0	0	0	0	0	0	0	0	0	0	0	0	0	0	0	0	0	0	0	0				
Lungs - pulmonary adenoma	0	0	0	0	0	0	0	0	0	0	0	0	0	0	0	0	0	0	0	0	0	0	0	0	0	0	0	0	0	0	0	0	0	0	0	0	0	0	0	0	0				
Heart - myocardial mineralization	0	0	0	0	0	0	0	2	0	0	0	0	0	0	0	0	0	0	0	0	0	0	0	0	0	0	0	0	0	0	0	0	0	0	0	0	0	0	0	0	0				
Salivary glands - inflammation	0	0	0	0	0	0	0	0	0	0	0	0	0	0	0	0	0	0	0	0	0	0	0	0	0	0	0	0	0	0	0	0	0	0	0	0	0	0	0	0	0				
Exorbital gland - inflammation	0	0	2	0	0	0	2	2	1	1	0	2	2	2	2	2	0	2	0	2	1	1	1	2	2	0	2	1	2	2	2	0	2	1	2	2	2	2	2	2	2	2	2		
Lymph nodes - lymphocytolysis	0	0	0	0	0	0	0	0	0	0	0	0	0	0	0	0	0	0	0	0	0	0	0	0	0	0	0	0	0	0	0	0	0	0	0	0	0	0	0	0	0				
Spleen - lymphoid hyperplasia	0	0	0	0	0	0	0	0	0	0	0	0	0	0	0	0	0	0	0	0	0	0	0	0	0	0	0	0	0	0	0	0	0	0	0	0	0	0	0	0	0				
Spleen - lymphocytolysis	0	0	0	0	0	0	0	0	0	0	0	0	0	0	0	0	0	0	0	0	0	0	0	0	0	0	0	0	0	0	0	0	0	0	0	0	0	0	0	0	0				
Spleen - extramedullary hematopoiesis	0	0	0	0	0	0	0	0	0	0	0	0	0	0	0	0	0	0	0	0	0	0	0	0	0	0	0	0	0	0	0	0	0	0	0	0	0	0	0	0	0				
Skin - inflammatory infiltrates	0	0	0	2	0	0	0	1	0	0	0	0	0	0	2	0	0	0	0	0	0	0	0	0	0	0	0	0	0	2	2	0	0	1	0	1	0	1	0	1	0				
Preputial gland - inflammatory infiltrates	NA	NA	NA	NA	NA	NA	NA	0	0	0	0	0	0	2	0	0	NA	NA	NA	NA	NA	0	2	0	2	0	0	NA	NA	NA	NA	NA	NA	0	0	0	0	NA	0	0	0	2			
Epididymis - inflammatory infiltrates	NA	NA	NA	NA	NA	NA	NA	0	0	0	0	0	0	0	0	0	0	0	0	0	0	0	0	0	0	0	0	0	0	0	0	0	0	0	0	0	0	0	0	0	0	0			
Uterus - endometrial cystic hyperplasia	0	0	0	0	0	0	0	0	0	0	NA	NA	NA	NA	0	0	0	0	0	0	NA	NA	NA	NA	NA	NA	NA	0	0	0	0	0	0	0	0	0	0	0	0	0	0	0			
Uterus - endometritis	0	0	0	0	0	0	0	0	0	0	0	0	0	0	0	0	0	0	0	0	0	0	0	0	0	0	0	0	0	0	0	0	0	0	0	0	0	0	0	0	0	0			
Uterus - inflammatory infiltrates	0	0	0	0	0	0	0	0	0	0	0	0	0	0	0	0	0	0	0	0	0	0	0	0	0	0	0	0	0	0	0	0	0	0	0	0	0	0	0	0	0	0			
Uterus - amyloid	0	0	0	0	0	0	0	0	0	0	0	0	0	0	0	0	0	0	0	0	0	0	0	0	0	0	0	0	0	0	0	0	0	0	0	0	0	0	0	0	0	0			
Uterus - myometrial pigment	0	0	0	0	0	0	0	0	0	0	0	0	0	0	0	0	0	0	0	0	0	0	0	0	0	0	0	0	0	0	0	0	0	0	0	0	0	0	0	0	0	0			
Uterus - luminal dilation	0	0	0	2	0	0	0	0	0	0	0	0	0	0	0	0	0	0	0	0	0	0	0	0	0	0	0	0	0	0	0	0	0	0	0	0	0	0	0	0	0	0			
Urinary bladder - inflammatory aggregates	0	0	0	0	0	0	0	0	0	0	0	0	0	0	0	0	0	0	0	0	0	0	0	0	0	0	0	0	0	0	0	0	0	0	0	0	0	0	0	0	0	0			
Bone marrow (sternum) - acidophilic macrophages	0	0	0	0	0	0	0	0	0	0	0	0	0	0	0	0	0	0	0	0	0	0	0	0	0	0	0	0	0	0	0	0	0	0	0	0	0	0	0	0	0	0			
Eyes - cataracts	0	0	0	0	0	0	0	0	0	0	0	0	0	0	0	0	0	0	0	0	0	0	0	0	0	0	0	0	0	0	0	0	0	0	0	0	0	0	0	0	0	0			
Middle ear - otitis	0	0	0	0	0	0	2	0	0	0	0	0	0	0	0	0	0	0	0	0	0	0	0	0	0	0	0	0	0	0	0	0	0	0	0	0	0	0	0	0	0	0			
Middle ear - mucoperiosteal proliferation	0	0	0	0	0	0	0	0	0	0	0	0	0	0	0	0	0	0	0	0	0	0	0	0	0	0	0	0	0	0	0	0	0	0	0	0	0	0	0	0	0	0			
Nasal sinuses - extracellular material	0	0	0	0	0	0	0	0	0	0	0	0	0	0	0	0	0	0	0	0	0	0	0	0	0	0	0	0	0	0	0	0	0	0	0	0	0	0	0	0	0	0			
Nasal sinuses - epithelial acidophilic droplets	0	0	0	0	0	0	0	0	0	0	0	0	0	0	0	0	0	0	0	0	0	0	0	0	0	0	0	0	0	0	0	0	0	0	0	0	0	0	0	0	0	0			
Nasal sinuses - sinusitis	0	0	0	0	0	0	0	0	0	0	0	0	0	0	0	0	0	0	0	0	0	0	0	0	0	0	0	0	0	0	0	0	0	0	0	0	0	0	0	0	0	0			
Brain (thalamus) - Hirano-like cytoplasmic crystals	0	0																																											

B

Lesion	PERK-A/A										PERK-A/B										PERK-B/B										Severity of change								
	Females					Males					Females					Males					Females					Males					Unremark	Change							
	1830	1821	2007	1915	2106	2200	2114	2119	2120	2125	2193	2194	1826	1827	1828	2008	2009	2010	1811	1812	1813	1817	1892	2006	1832	1959	1967	2002	2004	1819	1818	2110	2112	2005	1890	1891	Present	P	
Liver - hepatocytic swelling and clearing	2	1	1	1	1	2	3	3	3	3	3	3	3	3	3	3	1	1	1	2	3	3	2	3	2	2	2	2	2	3	3	2	2	2	3	3	0	0	
Liver - inflammatory portal infiltrates	1	2	1	3	3	1	2	2	2	3	2	2	1	1	1	3	1	1	2	2	3	1	2	2	1	2	2	1	2	1	2	0	1	1	1	1	1	2	2
Liver - extramedullary hematopoiesis	3	1	2	2	2	3	1	1	3	3	0	0	3	3	2	2	3	0	0	1	2	3	1	0	0	2	1	2	2	1	2	0	1	1	2	3	3	0	0
Liver - hepatic lipodiosis	0	0	0	0	0	0	0	0	0	0	0	0	0	0	0	0	0	0	0	0	0	0	0	0	0	0	0	0	0	0	2	0	0	0	0	0	0	0	
Liver - hepatocyte necrosis	0	0	0	0	0	0	0	0	0	0	0	0	0	0	0	0	0	0	0	0	0	0	0	0	0	0	0	0	0	0	0	0	0	1	0	2	0	0	
Liver - hepatocellular neoplasm																																						P	
Gallbladder - inflammation	3	0	0	2	0	1	0	0	0	0	3	0	0	0	0	0	0	0	3	0	0	0	0	2	0	0	2	0	0	0	0	0	0	0	0	0	0	2	0
Gallbladder - acidophilic droplets	4	0	0	0	0	0	0	0	0	0	0	0	0	0	0	0	0	0	4	0	0	0	0	0	0	0	3	0	0	0	0	0	0	0	0	0	0	0	0
Kidney - inflammatory infiltrates	4	2	1	2	3	3	2	2	3	2	2	0	1	2	2	3	2	3	0	3	3	2	3	3	2	1	2	2	2	1	0	2	2	2	3	3	0	0	
Pancreas - inflammatory infiltrates	2	0	0	2	0	2	0	0	0	0	3	0	1	2	3	1	1	2	0	0	2	0	2	0	1	1	1	2	0	1	2	2	1	0	1	0	1	1	1
Pancreas - vacuoles	1	2	2	2	2	1	1	1	1	1	3	2	3	2	2	2	2	0	2	0	1	1	2	1	1	2	2	1	2	2	0	1	2	1	1	2	2	0	
Pancreas - zymogen granule depletion	3	0	0	0	0	0	0	0	0	0	0	0	0	0	0	0	0	0	0	0	0	0	0	0	0	0	0	0	0	0	0	0	0	0	0	0	0	0	
Pancreas - atrophy	0	0	0	0	0	0	0	0	0	0	0	0	0	2	0	0	0	0	0	0	0	0	0	0	0	0	0	0	0	0	0	0	0	0	0	0	0	0	
Heart - myocardial mineralization	0	0	0	0	0	0	0	0	0	0	0	0	0	0	0	0	0	0	1	0	0	0	0	0	0	0	0	0	0	0	0	0	0	0	0	0	1	0	
Lungs - inflammatory aggregates	3	3	1	3	2	0	1	0	1	3	1	1	3	3	3	2	3	0	3	1	2	3	3	1	2	1	2	1	1	0	0	0	2	1	3	0	0	0	
Lungs - acidophilic macrophages	4	3	1	1	2	0	0	0	0	0	1	0	2	1	2	3	1	1	3	1	3	2	3	3	2	0	0	1	3	0	0	0	0	0	2	3	0	0	
Lungs - alveolar histiocytosis	0	0	0	0	0	0	0	0	0	1	0	0	0	0	0	0	0	0	0	0	0	0	0	0	0	0	0	0	0	0	0	0	1	0	0	0	0		
Lungs - pulmonary adenoma																																					P		
Salivary glands - inflammation	2	2	3	2	2	4	3	1	3	3	1	2	2	0	0	0	0	0	3	1	3	3	2	2	0	0	2	2	2	2	2	3	3	3	3	3	0	0	
Harderian glands - inflammation	0	0	0	1	2	0	0	0	0	0	0	0	0	2	2	2	1	0	2	0	0	0	0	1	0	2	0	0	2	0	0	0	2	0	2	0	0	1	
Lymph nodes - lymphocytolysis	0	0	0	0	0	0	0	0	0	0	0	0	0	0	0	0	0	0	0	0	0	0	0	0	0	0	0	0	0	0	0	0	0	0	0	0	0	0	
Spleen - lymphoid hyperplasia	2	0	2	0	0	2	3	2	3	3	0	0	0	1	0	0	1	1	3	0	0	0	0	0	0	0	0	0	0	0	0	0	0	0	0	0	0	0	
Spleen - lymphocytolysis	0	0	0	0	0	0	1	0	1	0	0	0	0	0	0	0	0	0	2	0	0	0	0	0	0	0	0	0	0	0	0	0	0	0	0	0	0	0	
Spleen - extramedullary hematopoiesis	2	2	1	1	1	1	1	1	2	1	1	1	1	1	2	1	1	1	1	1	1	1	1	1	1	1	2	1	1	1	1	1	1	1	1	1	1	1	
Skin - dermatitis	0	0	1	0	0	2	3	0	0	3	1	3	0	1	1	0	0	0	1	0	3	3	1	0	0	0	0	0	1	0	1	2	0	0	0	0	3	3	
Preputial gland - inflammatory infiltrates	N/A	N/A	N/A	N/A	N/A	N/A	1	1	0	1	2	0	N/A	N/A	N/A	N/A	N/A	0	0	2	2	0	2	N/A	N/A	N/A	N/A	N/A	N/A	N/A	0	1	1	0	0	0	0		
Epididymis - inflammatory infiltrates	N/A	N/A	N/A	N/A	N/A	N/A	0	1	0	1	0	0	N/A	N/A	N/A	N/A	N/A	0	0	0	0	0	0	0	0	N/A	N/A	N/A	N/A	N/A	0	0	0	0	0	0	0	0	
Uterus - endometrial cystic hyperplasia	0	0	1	1	3	0	N/A	N/A	N/A	N/A	N/A	N/A	0	0	1	2	0	0	N/A	N/A	N/A	N/A	N/A	N/A	2	0	0	0	0	0	0	0	0	0	0	0	0	0	0
Uterus - endometritis	0	0	0	0	0	0	N/A	N/A	N/A	N/A	N/A	N/A	0	0	0	1	0	0	N/A	N/A	N/A	N/A	N/A	N/A	2	0	1	0	0	0	1	N/A	N/A	N/A	N/A	N/A	N/A	N/A	N/A
Uterus - amyloid	0	0	0	0	0	0	N/A	N/A	N/A	N/A	N/A	N/A	0	0	0	0	0	0	N/A	N/A	N/A	N/A	N/A	N/A	0	0	0	0	0	0	3	N/A	N/A	N/A	N/A	N/A	N/A	N/A	
Urinary bladder - inflammatory aggregates	0	0	0	0	2	0	0	0	0	0	0	0	0	2	0	0	2	0	0	0	0	0	0	0	0	0	2	0	0	0	0	0	0	0	0	0	0		
Large intestine - protozoal overgrowth	0	0	0	0	0	3	3	1	3	0	0	0	0	0	0	0	0	0	0	0	0	0	0	0	1	0	3	3	3	0	0	0	3	3	0	3	1		
Bone marrow (sternum) - acidophilic macrophages	0	0	0	0	0	0	2	1	3	0	0	0	0	1	0	1	1	1	0	0	0	0	0	0	0	0	0	0	0	1	0	2	0	1	0	0	0		
Eyes - cataracts	0	0	0	0	0	0	0	0	0	0	0	0	0	0	0	0	0	0	0	0	0	0	0	0	0	0	0	0	0	0	0	0	0	0	0	0	0		
Middle ear - otitis	0	0	0	0	0	0	0	0	0	0	0	0	0	0	0	0	0	0	0	0	0	0	0	0	0	0	0	0	0	0	0	0	0	0	0	0	0		
Middle ear - mucopurulent proliferation																																					P		
Nasal sinuses - extracellular material	0	0	0	2	0	0	0	0	0	0	0	0	0	2	0	0	0	0	0	0	0	0	0	0	0	0	0	0	0	0	0	0	0	0	0	0	0		
Nasal sinuses - epithelial acidophilic droplets	0	0	0	2	1	0	0	0	0	0	0	0	0	0	0	2	1	0	0	0	0	0	0	0	0	0	0	0	0	0	0	0	0	0	0	0	0		
Nasal sinuses - sinusitis	0	0	0	0	0	0	0	0	0	0	0	0	0	0	0	0	0	0	0	0	0	0	0	0	0	0	0	0	0	0	0	0	0	0	0	0	0		
Brainstem - cerebellum - vacuolation	1	1	0	1	1	1	1	0	0	1	0	0	0	0	0	0	0	0	0	0	0	0	0	0	0	0	0	0	0	0	0	0	0	0	0	0	0		

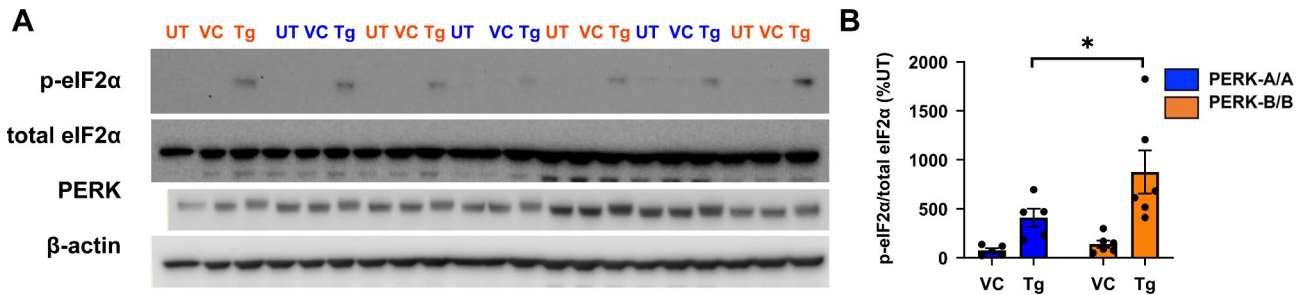


Fig. 4. ER-stress-induced PERK activity is higher in PERK-B/B-expressing MDMs than in PERK-A/A-expressing MDMs in vitro. **A.** Monocyte-derived macrophages isolated from PERK-A/A and PERK-B/B mice ($n = 5-6/\text{group}$) were treated with thapsigargin (Tg) or vehicle control (VC), and the protein levels of p-eIF2α, total eIF2α, PERK, and actin were determined with immunoblotting. Representative immunoblots are shown. **B.** Quantification of the immunoblots is shown. * $p < 0.05$, two-way repeated measures ANOVA with Sidak's test for multiple comparisons.

dependent effect on BIP and ATF4 protein levels in the liver homogenates of the vehicle and the tunicamycin-treated mice (Fig. 6e-f).

PERK-B/B mice exhibit increased tunicamycin-induced vulnerability in pancreas compared to PERK-A/A mice

Based on a large body of evidence indicating UPR activation as a contributor of neurodegeneration, we aimed to determine the mechanistic role of PERK-B/B in neurodegeneration. However, we did not detect tunicamycin-induced UPR activation in the CNS (Supplementary Fig S8a-c). To confirm that the dose and duration of tunicamycin were sufficient in inducing the UPR, we administered 6 mg/kg tunicamycin to mice over 72 h. The mortality rate, which was 33% at 48 h, reached 100% by 72 h. Importantly, despite the robust UPR activation detected in the liver (Supplementary Fig S8b), UPR activation was not evident in the CNS in our experimental paradigm, consistent with the poor CNS penetration of tunicamycin³⁹ (Supplementary Fig S8c).

ER stress, particularly PERK activation, is associated with pancreatic atrophy and dysfunction⁴⁰⁻⁴². Additionally, WRS and the PERK-B SNVs are associated with pancreatic insufficiency¹⁶ and prediabetes²⁰, respectively. In our analyses of the pancreatic homogenates from the tunicamycin-treated cohort of PERK-A/A and PERK-B/B mice, we observed higher eIF2α phosphorylation at baseline and following treatment with the vehicle DMSO. Unexpectedly, we observed a decrease in eIF2α phosphorylation in response to tunicamycin treatment in the PERK-B/B mice, which was absent in the PERK-A/A mice (Fig. 7a-c, Supplementary Fig S9). Meanwhile, the PERK protein levels remained comparable between the vehicle-treated PERK-A/A and PERK-B/B mice (Fig. 7d) whereas the BIP protein levels did not significantly differ between the tunicamycin-treated PERK-A/A and PERK-B/B mice (Fig. 7e). Acute and severe UPR, specifically PERK activation, is associated with the increased expression of the proapoptotic CHOP^{43,44} and cleaved-caspase 3⁴⁵⁻⁴⁹. In agreement, we observed significantly elevated cleaved caspase 3 levels in the pancreas in response to tunicamycin treatment and determined that this effect was dependent on the PERK genotype based on analysis with immunoblotting (Fig. 7f-g, Supplementary Fig S9) and immunohistochemistry (Supplementary Fig S10a-b). The pancreatic tissue of the tunicamycin-treated PERK-A/A and PERK-B/B mice displayed elevated *Chop* mRNA levels compared to the vehicle-treated PERK-A/A and PERK-B/B mice, and this effect was more pronounced with PERK-B/B (Fig. 7h-l).

Discussion

In this study, we use the novel triple knock-in PERK-B/B mouse model to provide insights into the in vivo and in vitro effects of disease risk-associated exonic PERK-B/B SNVs. Our analyses reveal that PERK-B/B is associated with increased PERK kinase activity in the liver and increased susceptibility to apoptosis in the pancreas, particularly under acute ER stress. These observations are further supported by the cell-free PERK kinase assay and data from MDM cultures, which also demonstrate elevated PERK activity in PERK-B/B cells, albeit with minimal functional consequences at acute timepoints. These findings hold significance as they shed light on the conflicting reports regarding the contribution of PERK-B SNVs to its kinase activity, which, in turn, can impact the development of therapeutic strategies for PERK-related disorders²⁷⁻²⁹.

Our data add to a growing body of evidence that common variants with small/medium effect size, such as the minor alleles of the exonic PERK-B SNVs, can contribute to pathologic mechanisms in the periphery and the CNS^{18-20,22-25,50}. Specifically, altered PERK activity is associated with increased risk and progression of pancreatic insufficiency⁵¹⁻⁵⁴, and hepatic dysfunction⁵⁵ and increased risk for neurodegeneration^{22,24,56}. Moreover, modulation of PERK activity has been demonstrated to be beneficial in the periphery⁵⁷ and the CNS⁵⁸⁻⁶⁵. Hence, there is a critical need to understand how the exonic PERK-B SNVs contribute to disease risk. To our knowledge, this is the first in vitro and in vivo model to investigate the role of PERK-B/B variants in pancreatic and hepatic disorders associated with ER stress, providing a platform to identify and optimize therapeutics in these disorders.

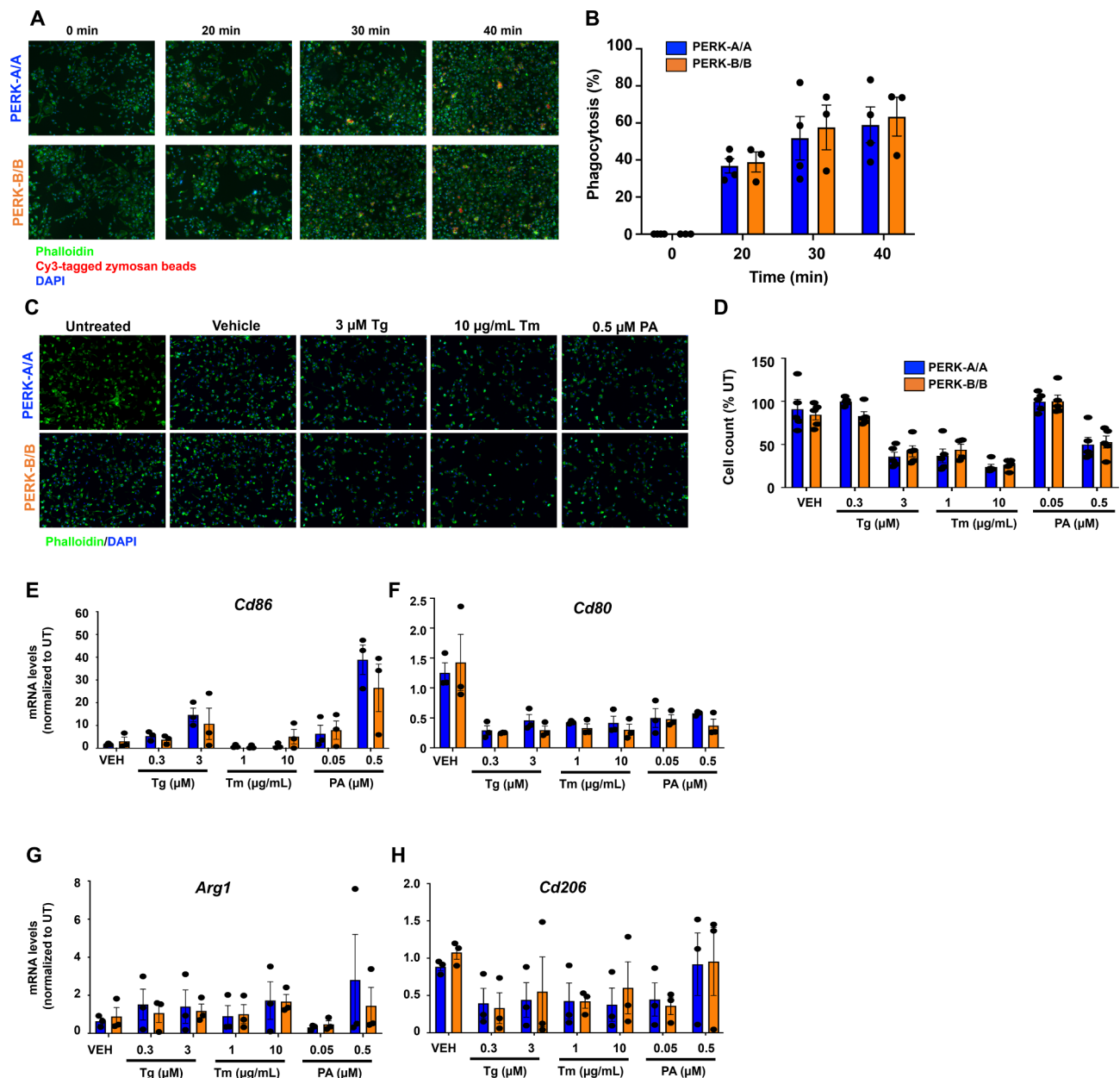


Fig. 5. Increased PERK activity in PERK-B/B MDMs is not associated with altered function in vitro. **A.** Cy3-tagged zymosan beads were added to PERK-A/A and PERK-B/B MDM cultures for 0–40 min to measure phagocytosis efficiency. Representative immunofluorescence images are shown. Phalloidin and DAPI were used to label macrophages and nuclei, respectively ($n = 3–6$ /group). **B.** Quantification of the number of bead-containing cells normalized to the total number of cells shows no significant difference between the groups. Two-way repeated measures ANOVA with Sidak's test for multiple comparisons. **C.** Cell survival of PERK-A/A and PERK-B/B MDMs was determined after 24 h of treatment with varying doses of tunicamycin (Tm), thapsigargin (Tg), or the PERK activator (PA) and compared to vehicle control (VC) and untreated control. Representative immunofluorescence images are shown. Phalloidin and DAPI were used to label macrophages and nuclei, respectively ($n = 3–4$ /group). **D.** Survival graphs of experiments shown in (C) are normalized to the untreated control. Two-way repeated measures ANOVA with Sidak's multiple comparisons, $*p < 0.05$. **E–H.** cDNA was isolated from PERK-A/A and PERK-B/B MDMs treated with varying doses of the ER stressors tunicamycin (Tm), thapsigargin (Tg), or the PERK activator (PA) for 12 h, and expression levels of *Cd86* (E), *Cd80* (F), *Arg1* (G), and *Cd206* (H) by qRT-PCR. Two-way repeated measures ANOVA with Sidak's multiple comparisons.

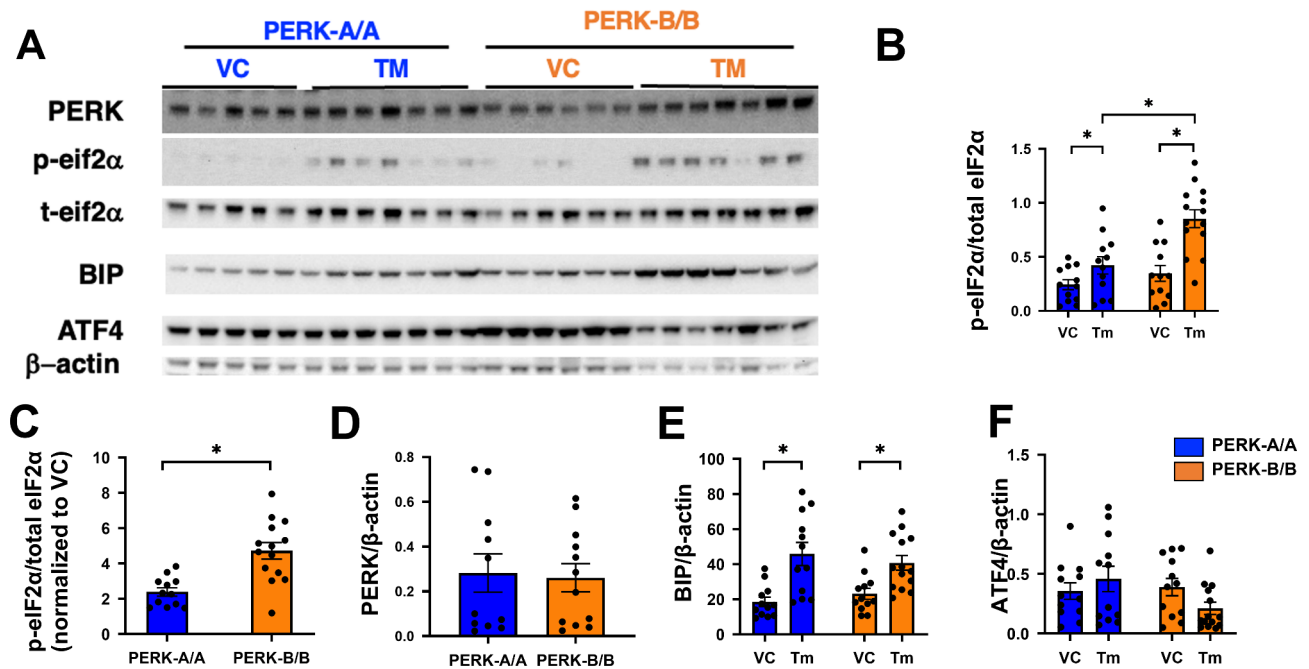


Fig. 6. ER stress-induced PERK activity is haplotype-dependent in the liver. **A.** Liver tissue homogenates from PERK-A/A and PERK-B/B mice treated with 0.5 mg/kg tunicamycin (Tm) or vehicle control (VC, $n = 10\text{--}14/\text{group}$) were analyzed by immunoblotting using antibodies against PERK, p-eIF2 α , total eIF2 α , BIP, and ATF4, with actin as the loading control. Representative blots are shown. **B.** Quantification of p-eIF2 α and total eIF2 α across all immunoblots. Two-way repeated measures ANOVA with Sidak's multiple comparisons, $*p < 0.05$. **C.** Quantification of p-eIF2 α and total eIF2 α across all immunoblots normalized to VC. Unpaired Student's t test, $*p < 0.05$. **D–F.** Quantification of PERK (**D**), BIP (**E**), and ATF4 (**F**). Two-way repeated measures ANOVA with Sidak's multiple comparisons, $*p < 0.05$.

First, we demonstrate that the PERK-B/B SNVs elevate PERK activity, both in cell-free conditions and within a cellular milieu. Data from previous *in vitro* studies elucidating the effects of PERK-B/B SNVs on PERK activity are conflicting. Liu et al. demonstrated that thapsigargin-induced PERK kinase activity was elevated in PERK-B/B-expressing lymphoblastoid cells²⁷. However, Yuan et al. reported PERK-B/B a hypomorph in mouse embryonic fibroblasts derived from patients with PSP²⁸. It is plausible that PERK activity is context-dependent, varying with stress severity and duration, cell type, and activity of other UPR players. Our data from the cell-free PERK kinase assay and MDM cultures expressing PERK-A/A or PERK-B/B not only support Liu et al., showing that PERK-B/B SNVs increase PERK kinase activity in a myeloid lineage cell type, but also confirm this observation in a cell-free system where the PERK levels are tightly controlled and potential contributions of modifying cofactors are absent.

We have developed our novel triple knock-in transgenic mouse model to elucidate the mechanisms underlying the reported associations of the minor alleles of PERK-B SNVs with pathologies in the periphery and the CNS^{18–25}, particularly their impact on PERK activity at baseline and during ER stress or disease contexts. We found no alterations in the PERK level or the baseline PERK activity, assessed by eIF2 α phosphorylation and changes in the levels of BIP and ATF4, both downstream signaling partners, in pancreas, liver, and brain of PERK-A/A and PERK-B/B mice. These findings are consistent with data from other *in vitro* studies, which indicate that the PERK-B/B SNVs do not induce changes in the expression level or the baseline kinase activity of PERK^{27,28}. To our knowledge, our study provides the first *in vivo* evidence on the impact of these SNVs on PERK expression and activity in a knock-in mouse model.

Our comprehensive histopathologic analyses to further characterize our mouse model and evaluate age-related pathologies revealed no discernible genotype or sex-dependent differences among the PERK-A/A, PERK-A/B, and PERK-B/B mice at 13 months of age. Intriguingly, the only subtle differences were increased acidic alveolar macrophages in PERK-A/B mice, increased lymphoid hyperplasia in PERK-A/A mice, and increased protozoal outgrowth in the colon of PERK-B/B mice. Based on the abundance of PERK haplotype A in about 65% of the global population, with no reports to date linking it to lymphoid hyperplasia in spleen, we believe these changes to be incidental. More definitive answers will require longer observation periods as well as prolonged stressors targeting spleen/lymphocytes to confirm and expound on this finding. Notwithstanding, changes observed in PERK-A/B mice might be an outcome of a mismatch in the active PERK dimer, which is a prerequisite for PERK kinase activity, and warrants further investigation. Notably, these differences were similar between the young and old cohorts. In this context, we leveraged the process of aging as a chronic and mild physiologic stressor, recognizing that aging is the strongest risk factor for various metabolic and neurodegenerative disorders. Our findings suggest that PERK-B SNVs may not act as independent drivers

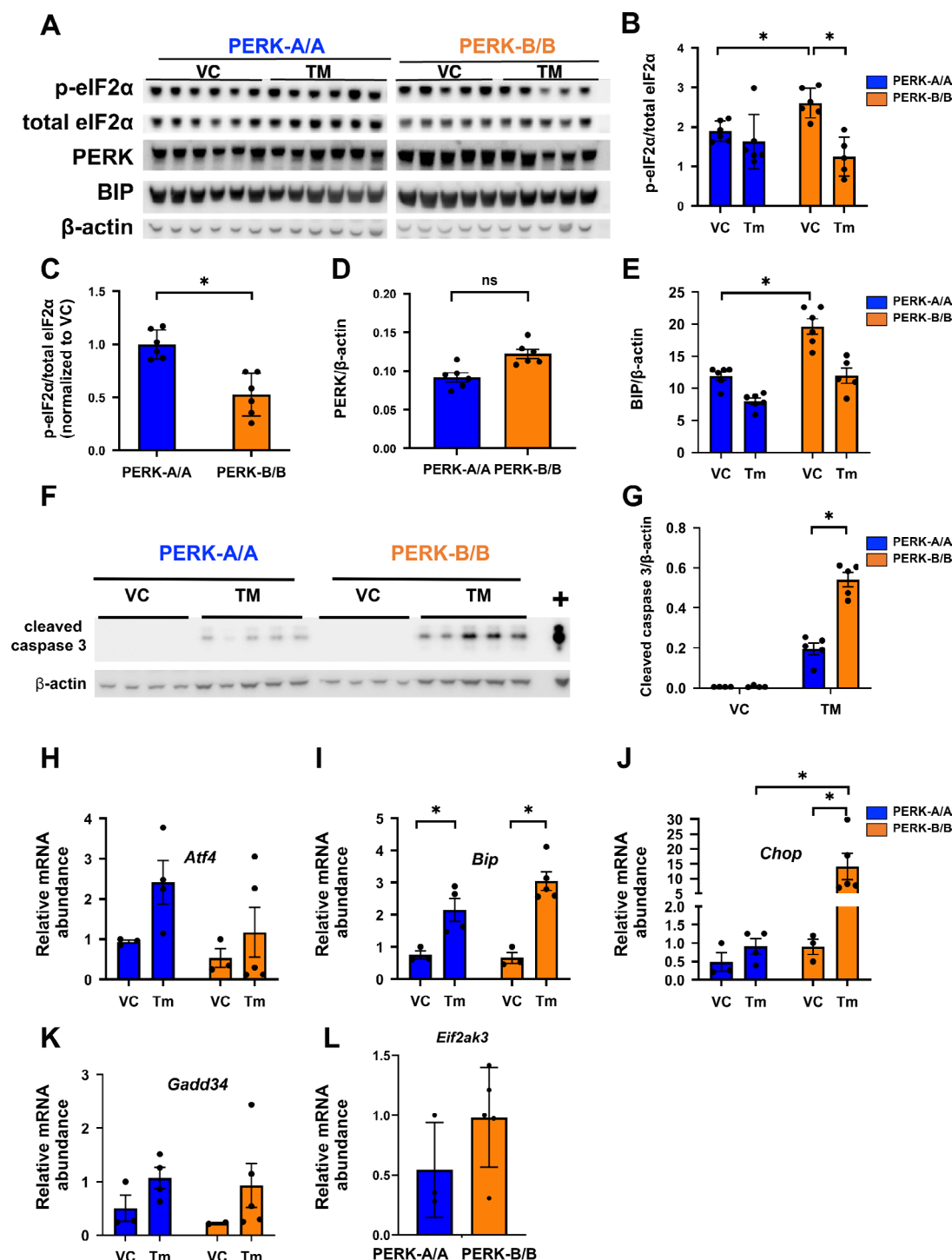


Fig. 7. PERK-B/B mice exhibit increased tunicamycin-induced vulnerability in pancreas compared to PERK-A/A mice. **A.** Pancreatic tissue homogenates from PERK-A/A and PERK-B/B mice treated with either 0.5 mg/kg tunicamycin (Tm) or vehicle control (VC, $n = 4-7$ /group) were analyzed by immunoblotting using antibodies against PERK, p-eIF2 α , total eIF2 α , and BIP, with actin as the loading control. Representative blots are shown. **B–E.** Quantification of the immunoblots are shown. Two-way ANOVA with Sidak's multiple comparison, * $p < 0.05$. **C.** Results of data shown in (A) normalized to the vehicle across all blots (unpaired t-test, * represents $p < 0.05$). **F.** Homogenates from (A) were also blotted for cleaved caspase 3 ($n = 4-5$). Representative blot is shown. **G.** Results of data shown in (F) are quantified across all blots (Two-way ANOVA with Sidak's multiple comparison test, ** represents $p < 0.01$). **H–L.** cDNA isolated from pancreatic tissue from PERK-A/A or PERK-B/B mice treated with vehicle or tunicamycin (0.5 μ g/g) for 24 h was analyzed for *Atf4* (H), *Bip* (I), *Chop* (J), *Gadd34* (K), and *Perk* (L) by qRT-PCR. Relative mRNA abundance is shown. Two-way ANOVA with Sidak's multiple comparisons. ** $p < 0.01$. $n = 3-4$ /group.

of aging-related pathologies but rather function as contributors in the presence of additional genetic and/or environmental factors. Indeed, approximately 28% of the global population harbor PERK-B in the absence of experiencing overt disease. The higher risk of late-onset AD reported in individuals with the PERK-B haplotype becomes evident only within the subpopulation of individuals carrying the *APOE* $\epsilon 4$ allele, the strongest genetic risk factor for AD identified to date²⁴. In our recent study demonstrating that people with HIV expressing PERK-B SNVs were at higher risk for neurocognitive impairment²⁵, HIV and antiretrovirals, both of which can induce the UPR^{66–70}, should be considered as sources of prolonged stress, providing further support to the concept of PERK-B SNVs as contributors, rather than drivers, of pathology. Our triple knock-in model will be valuable for further examination of this concept in chronic models of neurodegeneration and neuroinflammation.

Patients with WRS often experience early-onset diabetes, recurrent hepatic dysfunction episodes, and cognitive developmental delay^{16,17,36–38}. Therefore, we performed additional analyses of the pancreas, liver, and brain. Intriguingly, PERK kinase activity was elevated particularly in liver homogenates of PERK-B/B mice and was evident under acute ER stress, aligning with data from our cell-free kinase assay and in MDMs. As liver resident macrophages, Kupffer cells might contribute to observed pathologic consequences in WRS⁷¹. While we observed a genotype-dependent effect on eIF2 α phosphorylation but not on the protein levels of BIP or ATF4, this difference might be attributed to the influence of distinct, redundant pathways that regulate BIP and ATF4^{72,73}.

Unexpectedly, we observed decreased stress-induced PERK kinase activity in the pancreas of PERK-B/B mice. Given its increased susceptibility to ER stress^{59,74–76}, we postulated that the stress-induced decrease in PERK activity in the pancreas would indicate a commitment to apoptosis, which was supported by the increased staining for cleaved-caspase 3 observed by both immunoblotting and immunohistochemistry in the pancreatic tissue of both PERK-A/A and PERK-B/B mice treated with tunicamycin. Furthermore, the higher *Chop* mRNA levels observed in the pancreas of tunicamycin-treated PERK-B/B mice compared to the PERK-A/A mice align with a study by Nan et al., who reported the association of PERK-B SNVs with increased risk of prediabetes in a Chinese cohort²⁰ and suggest enhanced pancreatic vulnerability to ER stress-induced apoptosis associated with the PERK-B haplotype. Of note, we did not observe tunicamycin-induced UPR in the CNS, which was not unexpected given that tunicamycin does not cross the blood-brain barrier (BBB)³⁹, but one in vitro study reported that tunicamycin disrupts the BBB⁷⁷, raising the possibility that tunicamycin might exert indirect effects in the CNS unless intracerebroventricularly administered.

We observed higher PERK activity in PERK-B/B MDMs compared to PERK-A/A MDMs only after thapsigargin treatment. Given that the effect was observed at 2 h, it remains unclear whether the difference in PERK activity was transient or might be sustained over longer durations. Our assessments aimed to determine whether the difference in PERK activity between the two genotypes had functional consequences under baseline and stress conditions. Studies on MDMs in vitro revealed no differences in the kinetics of phagocytosis between the PERK-A/A and PERK-B/B MDMs, despite the observed difference in ER stress-induced kinase activity. Additionally, we evaluated the proinflammatory and anti-inflammatory phenotypes of MDMs, which are reported to be influenced by PERK^{32,33,35}. Interestingly, we observed an increase in the proinflammatory marker *Cd86*, a decrease in the proinflammatory marker *Cd80*, and a decrease in the anti-inflammatory marker *Cd206*, whereas the mRNA expression level of the anti-inflammatory marker *Arg1* remained relatively constant. These discordant data suggest the presence of a UPR-specific activation state that falls somewhere along the spectrum between the proinflammatory and anti-inflammatory phenotypes. Our in vitro data on MDMs contribute to the growing body of literature investigating the impact of PERK-B on its kinase activity^{27–29} and highlight a need to understand the complex impact of this difference on cellular function. Indeed, a study investigating astrocyte activation in response to ER stress established the presence of a UPR-specific activation state, which was distinct from the classic A1 and A2 activation states⁷⁸. Importantly, in this study the similar pattern observed in response to ER stress in the PERK-A/A and PERK-B/B MDMs suggest the presence of a shared UPR-related activation state in response to ER stress.

Severe and prolonged ER stress leads to cell death. To assess the potential differences in ER stress-induced cell survival associated with PERK haplotypes, we exposed both PERK-A/A and PERK-B/B MDMs to varying doses of thapsigargin, tunicamycin, and the PERK activator CCT020312. All three ER stressors induce UPR through distinct mechanisms. Thapsigargin inhibits the sarco-ER calcium ATPase pump, leading to cellular calcium dyshomeostasis, UPR activation, and, ultimately, apoptotic cell death⁷⁹. Tunicamycin inhibits N-glycosylation, disrupting protein maturation and rendering cells more susceptible to apoptosis^{80–83}. CCT020312 is a small-molecule PERK activator with potential anticancer therapeutic effects^{84,85}. In our experiments, both PERK-A/A and PERK-B/B MDMs exhibited sensitivity to high doses of thapsigargin, the PERK activator, and all doses of tunicamycin. The increased sensitivity to tunicamycin underscores the critical role of glycosylation in macrophage function and survival⁸⁶ and its importance in human health, more broadly⁸⁷. Conversely, the increased thapsigargin-induced PERK activity in PERK-B/B MDMs was not associated with observable functional changes, which might be attributed to the small/medium effect size associated with the PERK-B haplotype. Indeed, PERK-B has been associated with an elevated risk of neurocognitive impairment in individuals with HIV on antiretroviral therapy and the odds ratio of neurocognitive impairment for these relatively common variants within the study cohort is between 1.8 and 2.36 for both non-coding and coding SNVs associated with PERK-B²⁵. Given that approximately 28% of the global population carries these SNVs, it is plausible that these variants manifest as functional changes only under specific conditions, such as the presence of additional stressors, genetic risk factors, disease contexts, or exposure to environmental toxins. For instance, the association between PERK-B and AD is observed only within *APOE* $\epsilon 4$ carriers²⁴. Additionally, PERK-B increases the risk of neurocognitive impairment in individuals with HIV who are on antiretroviral therapy²⁵. In this case, HIV infection and antiretroviral drugs may act as sources of additional stressors, augmenting the

effects of PERK-B, underscoring the generalizable genomic concept that certain genetic risk variants such as PERK-B may act synergistically with other factors, revealing their functional impact in certain contexts.

The interpretation of the observed haplotype effects should take PERK abundance into account, given that PERK regulation also includes stabilization and degradation. In experiments where ER stress was induced (Figs. 4, 6, and 7), we also normalized the pElF2 α /total eIF2 α ratio to PERK protein levels (Supplementary Fig S11), which suggest that the haplotype effect of PERK-B* may be partially due to increased PERK abundance, as a result of increased stability or decreased degradation of PERK.

Critically, the prevalence of PERK-B is dependent on ancestry, with rates varying from 8% in individuals with African ancestry to 32% in those with European ancestry and approximately 50% in those with Asian ancestry⁵⁶. Notably, a majority of the studies investigating the impact of PERK-B on disease risk were conducted within Chinese cohorts^{18,20,23,24}. Although the consideration of ancestry is pivotal in studying disease risk, it is also essential to recognize that the complexity of human diseases cannot be fully replicated in mouse models. Furthermore, the current data are derived from homozygous PERK-A/A or PERK-B/B cultures and mice. However, investigating the impact of PERK-A/B would be physiologically relevant and can provide valuable insights. Additionally, our mouse model is designed to examine the three exonic SNVs associated with PERK-B and does not take into account three intronic SNVs that are in strong linkage disequilibrium with the three exonic SNVs; these intronic SNVs might potentially regulate protein expression and function through yet-unclear mechanisms.

Finally, although multiple studies have identified PERK as a potential therapeutic target for disorders affecting both the periphery and the CNS^{58–63,74,88}, pancreatic toxicity represents a significant limitation in most of these strategies^{59,74} based on studies showing that genetic *Eif2ak3* knockout in mice leads to apoptosis in pancreatic β -cells and the subsequent diabetic phenotype⁸⁹. Considering the diverse range of phenotypes linked to PERK-B in the pancreas and liver, including our findings, we propose that the PERK haplotypes should be taken into consideration during screening of potential therapeutic such as UPR modulators for their specific utility and efficacy in individuals harboring these commonly occurring *EIF2AK3* SNVs.

In conclusion, we have developed a novel mouse model to investigate the impact of PERK-B SNVs in pancreas, liver, and brain. Using a combination of cell-free, in vitro, and in vivo models, we illustrate that the SNVs associated with the PERK-B haplotype are associated with higher PERK activity in response to acute ER stress compared to the PERK-A haplotype in some cells and tissues. Importantly, these PERK-B-associated SNVs do not alter PERK expression or its kinase activity at baseline or following chronic mild stress in the form of age in either sex. These SNVs do not affect phagocytosis in MDMs in vitro, although altering the phenotype of following ER stress. These findings align with the observation that these SNVs exert a relatively modest/moderate effect size and exhibit functional consequences in the presence of additional environmental or genetic stressors. In summary, our novel model serves as a powerful tool to investigate the interactions of minor PERK alleles with disease modifiers, permitting improved approaches to leverage this model for therapeutic endpoints.

Materials and methods

Chemicals and reagents

Antibodies to the following targets were used: PERK (clone C33E10, catalog #3192), eIF2 α (clone L57A5, catalog #2103), pElF2 α (clone D9G8, catalog #3398), beta-actin (clone 8H10D10, catalog #3700), ATF4 (clone D4B8, catalog #11815), CHOP (clone L63F7, catalog#2895), cleaved caspase-3 (catalog #9661) from Cell Signaling Technology (Danvers, MA); and BIP (catalog #610978) from BD Transduction Laboratories (San Jose, CA). The following reagents were obtained from Thermo Fisher Scientific (Waltham, MA): Alexa Fluor 488 phalloidin (catalog #A12379), Alexa Flour 594-conjugated zymosan A bioparticles (catalog #Z23374), DAPI (catalog #D21490), tunicamycin (catalog #351610), target retrieval solution (catalog #S169984-2), TRIzol reagent (catalog #15596018), and TaqMan fast advanced master mix (catalog #4444557). The following reagents were from Cell Signaling Technology: RIPA buffer (catalog #9806) and 10% normal goat serum (catalog #5425). Recombinant mouse macrophage colony-stimulating factor (M-CSF; catalog #416-ML-500) was from R&D Systems (Minneapolis, MN), thapsigargin (catalog #11381) was from Tocris (Bristol, UK), the PERK activator CCT020312 (catalog #324879) was from Millipore Sigma (Burlington, MA), tyramide signal amplification kit (catalog #NEL700A001KT) was from Akoya Biosciences (Marlborough, MA), Vector NovaRED substrate kit, Peroxidase (HRP) (catalog #SK-4800) was from Vector Laboratories (Newark, CA), and RNeasy lipid tissue mini (catalog #74804) and RT2 first strand cDNA synthesis (catalog #330404) kits were from Qiagen (Hilden, Germany). For gene expression analyses, the following TaqMan assays (catalog #4331182, Thermo Fisher Scientific) were used: *Cd86* (Mm00444540_m1), *Cd80* (Mm00711660_m1), *Cd206* (Mm01329359_m1), *Arg1* (Mm00475988_m1), *Gapdh* (Mm99999915_g1), *Bip* (Mm00517691_m1), *Chop* (Mm01135937_g1), *Gadd34* (Mm01205601_g1), and *Atf4* (Mm00515325_g1).

Ethical considerations

All experimental protocols for animal studies were approved by the Institutional Animal Care and Use Committee at the University of Pennsylvania (protocol no. 806053) and conducted in accordance with the NIH guidelines and complied with ARRIVE guidelines for animal care and animal experimentation (<https://arriveguidelines.org>). Mice were deeply anesthetized with CO₂ in a chamber filled with 100% CO₂ at a fill rate of 30%–70% displacement/min. After observation of cessation of breathing for at least 2 min, euthanasia was confirmed by cervical dislocation.

Generation of the PERK-B mice

To generate the PERK-B/B mice, three single point mutations (S132C, R162Q, and S700A) were sequentially introduced in C57BL/6 mice using the proprietary CRISPR/Cas9 technology by Applied StemCell (Milpitas,

CA). Briefly, guide RNAs (gRNAs), single strand oligodeoxynucleotides (ssODNs), and Cas9 protein were microinjected into mouse embryos and gRNAs with the highest efficiency in directing cleavage in the mouse genome and minimal off-target profiles were selected. Based on the sequence of selected gRNAs, ssODN donors were synthesized to generate the desired mutations. The donor ssODNs served as DNA templates during homology-directed repair. Table 1 shows the gRNAs and ssODNs used to generate the novel triple knock-in PERK-B mice.

Protein purification and PERK kinase assay

For the PERK kinase assay, pcDNA plasmids encoding FLAG-tagged PERK-A or PERK-B were transfected into 293F cells (Thermo Fisher Scientific), which were harvested 48–72 h post-transfection and lysed in a buffer composed of 25 mM Tris–HCl, 150 mM NaCl, 1 mM EDTA, 1% NP-40, and 5% glycerol supplemented with Halt® phosphatase and protease inhibitor cocktail (Thermo Fisher Scientific). Cells were lysed on ice by vortexing, Dounce homogenization, and sonication for 45 s, including three cycles of 15-s sonication pulses with 15-s rest. The lysates were centrifuged at 30,000 g for 25 min in a refrigerated ultracentrifuge, and PERK-A and PERK-B were purified by running the cell lysates through an anti-FLAG resin (catalog #A36803; Thermo Fisher Scientific), eluted using 2.5 mg of 3 × FLAG peptide, followed by cleanup and concentration using Amicon 10-KDa MWCO ultrafiltration columns (catalog #UFC801024; Millipore Sigma). Purified proteins were quantified using the Bradford assay. The kinase buffer included 25 mM Tris–HCl, 5 mM beta-glycerophosphate, 2 mM DTT, 0.1 mM Na₃V0₄, 10 mM MgCl₂, and 100 μM ATP. Briefly, 100 ng of the FLAG-tagged full-length PERK-A or PERK-B was added into an eppendorf tube containing 7.3 ng of His-eIF2α (catalog #ADI-KPR-CP132-0200; Enzo Life Sciences, Farmingdale, NY) and the kinase buffer in a 50-μL reaction volume, yielding a 4.2 nM:16.8 nM substrate:enzyme molar ratio. The reaction was allowed to proceed at 37 °C for indicated time points, when the reaction was terminated with the addition of NuPAGE LDS buffer (Thermo Fisher Scientific), NuPAGE sample reducing agent (Thermo Fisher Scientific), and molecular grade water to reach a volume of 80 μL; 20μL of the final reaction mixture was used for immunoblotting.

In vivo treatments and tissue processing

Three-month-old male PERK-A/A and PERK-B/B mice were treated with tunicamycin for 24 h, as previously described^{90–95}. Briefly, tunicamycin was dissolved in 150 mM sterile dextrose and intraperitoneally injected at a dose of 0.5 μg/g bodyweight. After 24 h, the mice were euthanized and the tissues were harvested, flash frozen, and stored at –80 °C until use.

Immunoblotting

Tissue and cell lysates were prepared for immunoblotting, as previously described⁹⁶. Briefly, tissues and tissue cultures were homogenized and solubilized using a Dounce homogenizer in ice-cold RIPA buffer supplemented with Halt® protease and phosphatase inhibitor cocktail. Extracts were sonicated three times at 7-s intervals, with 10-s breaks, while on ice. The lysates were centrifuged at 12,000 g for 20 min at 4 °C. After determining the protein concentration of the supernatants, 10–20 μg of each sample was loaded into each lane of 4–12% Bis–Tris NuPAGE Novex gels (Thermo Fisher Scientific). For tissue cultures, 5–10 μg of total protein per condition was loaded into each lane of 4–12% Bis–Tris NuPAGE Novex gels. Next, the proteins were transferred to PVDF membranes, followed by blocking with Tris-buffered saline plus 0.1% Tween 20 (TBS-T) and 5% bovine serum albumin (BSA; Millipore Sigma) for 1 h at room temperature. The membranes were probed with indicated primary antibodies in TBS-T with 5% BSA overnight at 4 °C, followed by incubation with horseradish peroxidase-conjugated secondary antibodies (1:1000 in TBS-T with 5% BSA) for 30 min at room temperature. Bands were visualized by chemiluminescence using Luminata Classico ECL, and images were captured using film development or the ChemiDoc Touch imaging system (Bio-Rad, Hercules, CA). Equal loading and even transfer of samples were confirmed using beta-actin staining of the membranes. Densitometric analyses of band intensities were conducted using the ImageLab software version 6.0 (Bio-Rad), and all bands were normalized to beta-actin.

Complete pathologic analysis

Young (2–3 months) and old (13–14 months) PERK-A/A, PERK-A/B, and PERK-B/B mice, including both males and females, underwent complete pathologic examination. Briefly, following necropsy, organs were

	gRNA sequence (5' → 3')	ssODN sequence (5' → 3')
S132C	GGACGTGGGGTCTG GTTCCT	CACTTTAGATGGACGAATCGCTGCACTGGATGCCGAGAATGATGGGAAAAAGCAGTGGGATTGGACGTGGGGTCTGGTTGCTT GGTTTCATCTAGCCTCAGCAAGCCAGAGGTAAGGAAAGTCAAGTTGTATTGAGAATCGCTGCTGTGCTTGTGAGGC
R162Q	GAGACCTCTTCCAGT GGGAC	ATGAGGCTTTAAAAAGCGGCTTCTGTCTAGGTGTTTGGGAACAAGATGATCATCCCTCCCTGGATGGAGACCTTCCAGTGG GACCAGGACCGAGAGAGCATGGAGGCCGTCCCTTCACGGTGGAGTCCCTGCTCGAATCTTCTACAAGTTTGGAGATGA TGT
S700A	CCCCATCTGTTAAGA TCCGA	TCTGGCCACAGGAAATGCCACCGAGAAAGACCGACTTCTTTCAGGAGAAGGAGCTATGACTTCGATCTGCTCTTTTGTAGCGA AAGGATCCATTCTTCGGATCTTAACAGATGGGGATCCATCGGGCTAGGGGAGCTGAGCGGCCAGTCTGTGCTAAAAGGGGGAGA AACGAAAAGAGCTG

Table 1. gRNAs and ssODNs used to generate the novel triple knock-in PERK-B/B mice. Sequences of the PERK-B associated exonic SNPs are shown in bold, the gRNA recognition sites are shown in italic, and silent mutation is denoted in boldialic.

weighed, fixed with 10% formalin, and paraffin-embedded. Tissue sections stained with hematoxylin and eosin were evaluated by a certified veterinary comparative pathologist for the histopathologic assessment of organ-specific lesions, as described previously^{52–56}. Lesions were scored on a scale of 0, 1, 2, 3, and 4 for unremarkable, minimal, mild, moderate, and severe changes, respectively.

MDM culture

Monocytes isolated from bone marrow were differentiated into MDMs, as previously described⁹⁷. Briefly, femurs of 3-month-old male mice were isolated, and resident monocytes were flushed using a 30-gauge needle with 5 mL of MDM medium (RPMI 1640 with 10% fetal bovine serum, 1% penicillin/streptomycin, and 20 ng/mL gentamicin). The collected cells were strained using a 40- μ m filter, plated at a density of 0.5 million cells/mL on CellBind® plates (Thermo Fisher Scientific), and differentiated into MDMs using 20 ng/mL M-CSF. Twenty-four hours before treatments, 100% of the culture medium was replenished to remove M-CSF.

Phagocytosis assay and flow cytometry

Phagocytosis assay and flow cytometry were used to characterize MDMs, as described⁹⁷. For the phagocytosis assay, fluorescently labeled zymosan beads were coated with the opsonizing solution provided with the kit in HBSS at 37 °C for 1 h. After washes to remove residual opsonizing reagent, the beads were added to the MDMs for indicated time points, when the assay was stopped by removing the medium and washing cells with ice-cold phosphate-buffered saline (PBS), followed by fixation using 4% paraformaldehyde. The fixed cells were permeabilized and stained with phalloidin (1:400) and DAPI (1:1000) for immunofluorescence analysis. For flow cytometric analysis, MDMs were trypsinized using 0.5% trypsin-EDTA for 30 min at 37 °C, and the reaction was neutralized using an equal volume of MDM growth media, and cells pelleted at 200 g for 5 min at 4 °C. The pellets were resuspended, and an appropriate number of cells were blocked in BioLegend 1:4000 CD16/32 block (Cat. No. 101302) for 10 min. After blocking, cells were incubated in primary antibodies (F4/80 and CD11b) for 30 min in the dark, all at 1:400. After the incubation, cells were spun down at 200 g at 4 °C for 5 min and resuspended in RMPI. Samples are then analyzed on a BD LSRFortessa device, analyzed according to the software, and compensated accordingly.

Immunostaining

Immunofluorescence was performed as previously described⁹⁶. Primary MDM cultures were prepared and stained as follows. After treatment, cells were rinsed with PBS and fixed with 4% paraformaldehyde for 20 min. Cells were then rinsed twice in PBS and three times in PBS-T, followed by a 60 min incubation with a blocking/permeabilization solution containing 0.2% BSA and 0.1% Triton-X in PBS. Cells were rinsed three times in PBS-T and incubated with phalloidin diluted at 1:400 in normal antibody diluent for 30 min at room temperature. After three washes in PBS-T and two additional washes in PBS, cells were imaged using a Keyence BZ-X-700 digital fluorescent microscope affixed with UV, FITC, Cy3, and Cy5 filters. Images captured at 10 \times magnification were analyzed with the Keyence BZ-X software to quantify the number of macrophages, averaged across 25 fields/well, with 2–4 wells/treatment conditions for each biologic replicate. For immunohistochemistry (IHC), pancreas tissue was fixed, paraffin-embedded, and 5 μ m slices were used for IHC. The slides were incubated at 55 °C overnight, following rehydration, which consisted of sequential 5–10-min incubations in histoclear, 100% ethanol, 95% ethanol, 90% ethanol, 70% ethanol, and 3% hydrogen peroxide in methanol, and water. The slides were then heated at 95 °C for 20–30 min in a target retrieval solution for antigen retrieval, followed by PBS washes and blocked for 60 min in 10% normal goat serum. The slides were incubated with primary antibody for cleaved caspase (at a 1:100 dilution) overnight at 4C, followed by a tyramide signal amplification per the manufacturer's instructions. The amplified signal for cleaved caspase 3 was developed using a chromogenic substrate and counterstained with hematoxylin per the manufacturer's instructions.

Real-time polymerase chain reaction

Treated cells or tissue were harvested in TRIzol reagent, and RNA was extracted using the RNeasy lipid tissue mini kit per manufacturer's protocol. Using a nanodrop spectrophotometer, RNA quality was assessed using the A260/280 and A260/230 ratios. Equal amounts of RNA were used to synthesize cDNA using the RT2 first strand cDNA synthesis kit. No reverse transcription (RT) and no template controls were used. The cDNA was diluted 1:10 and gene expression was analyzed using TaqMan assays for *Cd80*, *Cd86*, *Cd206*, *Arg1*, *Bip*, *Chop*, *Gadd34*, and *Atf4* while using *Gapdh* as the housekeeping control.

cDNA was mixed with TaqMan assays, TaqMan fast advanced master mix, and water in a 96-well qPCR plate, sealed with an optical adhesive film. All samples were loaded in at least three technical replicates for qPCR analysis, with a no-RT and no-template control. The samples were analyzed on a Quantstudio 3, and gene expression was analyzed using $\Delta\Delta C_t$ method.

Data availability

The datasets used and/or analyzed during the current study are available from the corresponding author on reasonable request.

Received: 8 April 2024; Accepted: 25 September 2024

Published online: 11 October 2024

References

- Gallagher, M. D. & Chen-Plotkin, A. S. The post-GWAS era: From association to function. *Am. J. Hum. Genet.* **102**, 717–730 (2018).
- Spain, S. L. & Barrett, J. C. Strategies for fine-mapping complex traits. *Hum. Mol. Genet.* **24**, R111–R119 (2015).
- Boyle, E. A., Li, Y. I. & Pritchard, J. K. An expanded view of complex traits: from polygenic to omnigenic. *Cell* **169**, 1177–1186 (2017).
- Bond, S., Lopez-Lloreda, C., Gannon, P. J., Akay-Espinoza, C. & Jordan-Sciutto, K. L. The integrated stress response and phosphorylated eukaryotic initiation factor 2 α in neurodegeneration. *J. Neuropathol. Exp. Neurol.* <https://doi.org/10.1093/jnen/nlz129> (2020).
- Walter, P. & Ron, D. The unfolded protein response: From stress pathway to homeostatic regulation. *Science* **334**, 1081–1086 (2011).
- Donnelly, N., Gorman, A. M., Gupta, S. & Samali, A. The eIF2 α kinases: Their structures and functions. *Cell. Mol. Life Sci.* **70**, 3493–3511 (2013).
- Wek, R. C. & Cavener, D. R. Translational control and the unfolded protein response. *Antioxid. Redox Signal.* **9**, 2357–2372 (2007).
- Hinnebusch, A. G. Evidence for translational regulation of the activator of general amino acid control in yeast. *Proc. Natl. Acad. Sci.* **81**, 6442–6446 (1984).
- Wethmar, K., Smink, J. J. & Leutz, A. Upstream open reading frames: molecular switches in (patho) physiology. *Bioessays* **32**, 885–893 (2010).
- Erguler, K., Pieri, M. & Deltas, C. A mathematical model of the unfolded protein stress response reveals the decision mechanism for recovery, adaptation and apoptosis. *BMC Syst. Biol.* **7**, 16. <https://doi.org/10.1186/1752-0509-7-16> (2013).
- Chakrabarti, A., Aboulmouna, L. & Varner, J. Mechanistic modeling and analysis of the mammalian unfolded protein response. *BioRxiv*, 060020 (2016).
- Bchir, W. et al. The eIF2 α /ATF4 pathway is essential for stress-induced autophagy gene expression. *Nucleic Acids Res.* **41**, 7683–7699. <https://doi.org/10.1093/nar/gkt563> (2013).
- Dinkova-Kostova, A. T. & Abramov, A. Y. The emerging role of Nrf2 in mitochondrial function. *Free Radic. Biol. Med.* **88**, 179–188. <https://doi.org/10.1016/j.freeradbiomed.2015.04.036> (2015).
- Sarcinelli, C. et al. ATF4-dependent NRF2 transcriptional regulation promotes antioxidant protection during endoplasmic reticulum stress. *Cancers* **12**, 569 (2020).
- Moncan, M. et al. Regulation of lipid metabolism by the unfolded protein response. *J. Cell. Mol. Med.* **25**, 1359–1370. <https://doi.org/10.1111/jcmm.16255> (2021).
- Delépine, M. et al. EIF2AK3, encoding translation initiation factor 2- α kinase 3, is mutated in patients with Wolcott-Rallison syndrome. *Nat. Genet.* **25**, 406–409 (2000).
- Bruch, J. et al. Early neurodegeneration in the brain of a child without functional PKR-like endoplasmic reticulum kinase. *J. Neuropathol. Exp. Neurol.* **74**, 850–857 (2015).
- Liu, Y. et al. ER stress-related genes EIF2AK3, HSPA5, and DDIT3 polymorphisms are associated with risk of lung cancer. *Front. Genet.* **13**, 938787 (2022).
- Haddadi, S. et al. PKR-like ER kinase (PERK) haplotypes are associated with depressive symptoms in people with HIV. *J. Neurol. Psychol.* **10** (2023).
- Nan, F. et al. Common variants in PERK, JNK, BIP and XBP1 genes are associated with the risk of prediabetes or diabetes-related phenotypes in a Chinese population. *Chin. Med. J.* **127**, 2438–2444 (2014).
- Stutzbach, L. D. et al. The unfolded protein response is activated in disease-affected brain regions in progressive supranuclear palsy and Alzheimer's disease. *Acta Neuropathol. Commun.* **1**, 31. <https://doi.org/10.1186/2051-5960-1-31> (2013).
- Hoglinger, G. U. et al. Identification of common variants influencing risk of the tauopathy progressive supranuclear palsy. *Nat. Genet.* **43**, 699–705. <https://doi.org/10.1038/ng.859> (2011).
- Zhao, Q. et al. Correlation between single nucleotide polymorphism of EIF2AK3 gene and the efficacy of recombinant human growth hormone in children with growth hormone deficiency. *Chin. J. Endocrinol. Metab.* 492–498 (2020).
- Liu, Q.-Y. et al. An exploratory study on STX6, MOBP, MAPT, and EIF2AK3 and late-onset Alzheimer's disease. *Neurobiology of Aging* **34**, 1519. e1513–1519. e1517 (2013).
- Akay-Espinoza, C. et al. Genetic variations in EIF2AK3 are associated with neurocognitive impairment in people living with HIV. *medRxiv* (2022).
- Ferrari, R. et al. Assessment of common variability and expression quantitative trait loci for genome-wide associations for progressive supranuclear palsy. *Neurobiol. Aging* **35**, 1514. e1511–1514. e1512 (2014).
- Liu, J. et al. A functional haplotype in EIF2AK3, an ER stress sensor, is associated with lower bone mineral density. *J. Bone Min. Res.* **27**, 331–341. <https://doi.org/10.1002/jbmr.549> (2012).
- Yuan, S. H. et al. Tauopathy-associated PERK alleles are functional hypomorphs that increase neuronal vulnerability to ER stress. *Hum. Mol. Genet.* **27**, 3951–3963 (2018).
- Lenh, D. *Phenotypic Manifestations of EIF2AK3 Haplotype B Genotypes in Fibroblasts Derived from Patients with Progressive Supranuclear Palsy* 10615146 thesis (University of California, 2017).
- Thastrup, O., Cullen, P. J., Dröbak, B. K., Hanley, M. R. & Dawson, A. P. Thapsigargin, a tumor promoter, discharges intracellular Ca²⁺ stores by specific inhibition of the endoplasmic reticulum Ca²⁺ (+)-ATPase. *Proc. Natl. Acad. Sci.* **87**, 2466–2470 (1990).
- Raines, C., Radcliffe, O. & Treisman, G. J. Neurologic and psychiatric complications of antiretroviral agents. *J. Assoc. Nurses AIDS Care* **16**, 35–48 (2005).
- Pratap, U. P. & Vadlamudi, R. K. PERK promotes immunosuppressive M2 macrophage phenotype by metabolic reprogramming and epigenetic modifications through the PERK-ATF4-PSAT1 axis. *Immunometabolism (Cobham Surrey, England)* **4**, e00007 (2022).
- Yang, F. et al. ER-stress regulates macrophage polarization through pancreatic EIF-2 α kinase. *Cell. Immunol.* **336**, 40–47 (2019).
- Guthrie, L. N. et al. Attenuation of PKR-like ER kinase (PERK) signaling selectively controls endoplasmic reticulum stress-induced inflammation without compromising immunological responses. *J. Biol. Chem.* **291**, 15830–15840 (2016).
- Lim, Y.-J. et al. Roles of endoplasmic reticulum stress-mediated apoptosis in M1-polarized macrophages during mycobacterial infections. *Sci. Rep.* **6**, 37211 (2016).
- Reis, A. F. et al. Two novel mutations in the EIF2AK3 gene in children with Wolcott-Rallison syndrome. *Pediatric Diabetes* **12**, 187–191 (2011).
- Brickwood, S. et al. Wolcott-Rallison syndrome: pathogenic insights into neonatal diabetes from new mutation and expression studies of EIF2AK3. *J. Med. Genet.* **40**, 685–689 (2003).
- Julier, C. & Nicolino, M. Wolcott-Rallison syndrome. *Orphanet J. Rare Dis.* **5**, 1–13 (2010).
- Crider, A. et al. Estrogen receptor beta agonist attenuates endoplasmic reticulum stress-induced changes in social behavior and brain connectivity in mice. *Mol. Neurobiol.* **55**, 7606–7618. <https://doi.org/10.1007/s12035-018-0929-8> (2018).
- Sah, R. P. et al. Endoplasmic reticulum stress is chronically activated in chronic pancreatitis. *J. Biol. Chem.* **289**, 27551–27561 (2014).
- Papa, F. R. Endoplasmic reticulum stress, pancreatic β -cell degeneration, and diabetes. *Cold Spring Harbor Perspect. Med.* a007666 (2012).

42. Kubisch, C. H. et al. Early activation of endoplasmic reticulum stress is associated with arginine-induced acute pancreatitis. *Am. J. Physiol. Gastrointest. Liver Physiol.* **291**, G238–G245 (2006).
43. Rozpedek, W. et al. The role of the PERK/eIF2 α /ATF4/CHOP signaling pathway in tumor progression during endoplasmic reticulum stress. *Curr. Mol. Med.* **16**, 533–544 (2016).
44. Nishitoh, H. CHOP is a multifunctional transcription factor in the ER stress response. *J. Biochem.* **151**, 217–219 (2012).
45. Hitomi, J. et al. Apoptosis induced by endoplasmic reticulum stress depends on activation of caspase-3 via caspase-12. *Neurosci. Lett.* **357**, 127–130 (2004).
46. Lim, E. J., Heo, J. & Kim, Y.-H. Tunicamycin promotes apoptosis in leukemia cells through ROS generation and downregulation of survivin expression. *Apoptosis* **20**, 1087–1098 (2015).
47. Masud, A. et al. Endoplasmic reticulum stress-induced death of mouse embryonic fibroblasts requires the intrinsic pathway of apoptosis. *J. Biol. Chem.* **282**, 14132–14139 (2007).
48. Wei, M. C. et al. Proapoptotic BAX and BAK: a requisite gateway to mitochondrial dysfunction and death. *Science* **292**, 727–730 (2001).
49. Benítez-Rangel, E. et al. Caspase-3 activation correlates with the initial mitochondrial membrane depolarization in neonatal cerebellar granule neurons. *Front. Cell Dev. Biol.* **8**, 544 (2020).
50. Wong, T. H. et al. EIF2AK3 variants in Dutch patients with Alzheimer's disease. *Neurobiol. Aging* **73**, 229 e211–229 e218, <https://doi.org/10.1016/j.neurobiolaging.2018.08.016> (2019).
51. Marfour, I. et al. Expression of endoplasmic reticulum stress markers in the islets of patients with type 1 diabetes. *Diabetologia* **55**, 2417–2420 (2012).
52. Engin, F. et al. Restoration of the unfolded protein response in pancreatic β cells protects mice against type 1 diabetes. *Sci. Transl. Med.* **5**, 211ra156–211ra156 (2013).
53. Laybutt, D. et al. Endoplasmic reticulum stress contributes to beta cell apoptosis in type 2 diabetes. *Diabetologia* **50**, 752–763 (2007).
54. Engin, F., Nguyen, T., Yermalovich, A. & Hotamisligil, G. S. Aberrant islet unfolded protein response in type 2 diabetes. *Sci. Rep.* **4**, 4054 (2014).
55. Liu, X. & Green, R. M. Endoplasmic reticulum stress and liver diseases. *Liver Res.* **3**, 55–64 (2019).
56. Park, G. et al. Neurodegeneration risk factor, EIF2AK3 (PERK), influences tau protein aggregation. *J. Biol. Chem.* **299** (2023).
57. Moon, S. et al. Glucolipotoxicity suppressed autophagy and insulin contents in human islets, and attenuation of PERK activity enhanced them in an ATG7-dependent manner. *Diabetes Metab. J.* (2023).
58. Ma, T. et al. Suppression of eIF2 α kinases alleviates Alzheimer's disease-related plasticity and memory deficits. *Nat. Neurosci.* **16**, 1299 (2013).
59. Moreno, J. A. et al. Oral treatment targeting the unfolded protein response prevents neurodegeneration and clinical disease in prion-infected mice. *Sci. Transl. Med.* **5**, 206ra138. <https://doi.org/10.1126/scitranslmed.3006767> (2013).
60. Radford, H., Moreno, J. A., Verity, N., Halliday, M. & Mallucci, G. R. PERK inhibition prevents tau-mediated neurodegeneration in a mouse model of frontotemporal dementia. *Acta Neuropathol.* **130**, 633–642. <https://doi.org/10.1007/s00401-015-1487-z> (2015).
61. Halliday, M. et al. Repurposed drugs targeting eIF2 α -P-mediated translational repression prevent neurodegeneration in mice. *Brain* **140**, 1768–1783 (2017).
62. Espina, M. et al. The GRP78-PERK axis contributes to memory and synaptic impairments in Huntington's disease R6/1 mice. *Neurobiol. Dis.* **184**, 106225 (2023).
63. Ganz, J. et al. A novel specific PERK activator reduces toxicity and extends survival in Huntington's disease models. *Sci. Rep.* **10**, 1–15 (2020).
64. Bruch, J. et al. PERK activation mitigates tau pathology in vitro and in vivo. *EMBO Mol. Med.* **9**, 371–384 (2017).
65. Celardo, I. et al. Mitofusin-mediated ER stress triggers neurodegeneration in pink1/parkin models of Parkinson's disease. *Cell Death Dis.* **7**, e2271–e2271 (2016).
66. Gannon, P. J. et al. HIV protease inhibitors alter amyloid precursor protein processing via beta-site amyloid precursor protein cleaving enzyme-1 translational up-regulation. *Am. J. Pathol.* **187**, 91–109. <https://doi.org/10.1016/j.ajpath.2016.09.006> (2017).
67. Akay, C. et al. Antiretroviral drugs induce oxidative stress and neuronal damage in the central nervous system. *J. Neurovirol.* **20**, 39–53. <https://doi.org/10.1007/s13365-013-0227-1> (2014).
68. Akay, C. et al. Activation status of integrated stress response pathways in neurones and astrocytes of HIV-associated neurocognitive disorders (HAND) cortex. *Neuropathol. Appl. Neurobiol.* **38**, 175–200. <https://doi.org/10.1111/j.1365-2990.2011.01215.x> (2012).
69. Roth, L. M. et al. Differential effects of integrase strand transfer inhibitors, elvitegravir and raltegravir, on oligodendrocyte maturation: A role for the integrated stress response. *Glia* **69**, 362–376 (2021).
70. Lindl, K. A., Akay, C., Wang, Y., White, M. G. & Jordan-Sciutto, K. L. Expression of the endoplasmic reticulum stress response marker, BiP, in the central nervous system of HIV-positive individuals. *Neuropathol. Appl. Neurobiol.* **33**, 658–669. <https://doi.org/10.1111/j.1365-2990.2007.00866.x> (2007).
71. Habeb, A. M. et al. Liver disease and other comorbidities in Wolcott-Rallison syndrome: Different phenotype and variable associations in a large cohort. *Horm. Res. Paediatr.* **83**, 190–197 (2015).
72. Gong, J. et al. Molecular signal networks and regulating mechanisms of the unfolded protein response. *J. Zhejiang Univ. Sci. B* **18**, 1–14. <https://doi.org/10.1631/jzus.B1600043> (2017).
73. Neill, G. & Masson, G. R. A stay of execution: ATF4 regulation and potential outcomes for the integrated stress response. *Front. Mol. Neurosci.* <https://doi.org/10.3389/fnmol.2023.1112253> (2023).
74. Moreno, J. A. et al. Sustained translational repression by eIF2 α -P mediates prion neurodegeneration. *Nature* **485**, 507–511 (2012).
75. Iida, K., Li, Y., McGrath, B. C., Frank, A. & Cavener, D. R. PERK eIF2 α kinase is required to regulate the viability of the exocrine pancreas in mice. *BMC Cell Biol.* **8**, 1–16 (2007).
76. Gao, Y. et al. PERK is required in the adult pancreas and is essential for maintenance of glucose homeostasis. *Mol. Cell Biol.* (2012).
77. Finniet, J. & O'Shea, J. Effect of tunicamycin on the blood-brain barrier and on endothelial cells in vitro. *J. Comp. Pathol.* **102**, 363–374 (1990).
78. Smith, H. L. et al. Astrocyte unfolded protein response induces a specific reactivity state that causes non-cell-autonomous neuronal degeneration. *Neuron* **105**, 855–866 (2020).
79. Sehgal, P. et al. Inhibition of the sarco/endoplasmic reticulum (ER) Ca²⁺-ATPase by thapsigargin analogs induces cell death via ER Ca²⁺ depletion and the unfolded protein response. *J. Biol. Chem.* **292**, 19656–19673 (2017).
80. Jung, Y.-H., Lim, E. J., Heo, J., Kwon, T. K. & Kim, Y.-H. Tunicamycin sensitizes human prostate cells to TRAIL-induced apoptosis by upregulation of TRAIL receptors and downregulation of cIAP2. *Int. J. Oncol.* **40**, 1941–1948 (2012).
81. Azim, M. & Surani, H. Glycoprotein synthesis and inhibition of glycosylation by tunicamycin in preimplantation mouse embryos: compaction and trophoblast adhesion. *Cell* **18**, 217–227 (1979).
82. Hakulinen, J. K. et al. MraY-antibiotic complex reveals details of tunicamycin mode of action. *Nat. Chem. Biol.* **13**, 265–267 (2017).
83. Yoo, J. et al. GlcNAc-1-P-transferase-tunicamycin complex structure reveals basis for inhibition of N-glycosylation. *Nat. Struct. Mol. Biol.* **25**, 217–224 (2018).
84. Stockwell, S. R. et al. Mechanism-based screen for G1/S checkpoint activators identifies a selective activator of EIF2AK3/PERK signalling. *PLoS One* **7**, e28568 (2012).
85. Lei, Y., He, L., Yan, C., Wang, Y. & Lv, G. PERK activation by CCT020312 chemosensitizes colorectal cancer through inducing apoptosis regulated by ER stress. *Biochem. Biophys. Res. Commun.* **557**, 316–322 (2021).

86. Mantuano, N. R., Oliveira-Nunes, M. C., Alisson-Silva, F., Dias, W. B. & Todeschini, A. R. Emerging role of glycosylation in the polarization of tumor-associated macrophages. *Pharmacol. Res.* **146**, 104285 (2019).
87. Reily, C., Stewart, T. J., Renfrow, M. B. & Novak, J. Glycosylation in health and disease. *Nat. Rev. Nephrol.* **15**, 346–366 (2019).
88. Halliday, M. et al. Partial restoration of protein synthesis rates by the small molecule ISRIB prevents neurodegeneration without pancreatic toxicity. *Cell Death Dis.* **6**, e1672. <https://doi.org/10.1038/cddis.2015.49> (2015).
89. Ladiges, W. C. et al. Pancreatic β -cell failure and diabetes in mice with a deletion mutation of the endoplasmic reticulum molecular chaperone gene P58IPK. *Diabetes* **54**, 1074–1081 (2005).
90. Feng, B. et al. Endoplasmic reticulum stress inducer tunicamycin alters hepatic energy homeostasis in mice. *Int. J. Mol. Sci.* **18**, 1710 (2017).
91. Jo, H. et al. Endoplasmic reticulum stress induces hepatic steatosis via increased expression of the hepatic very low-density lipoprotein receptor. *Hepatology* **57**, 1366–1377 (2013).
92. Gomez, J. A. & Rutkowski, D. T. Experimental reconstitution of chronic ER stress in the liver reveals feedback suppression of BiP mRNA expression. *Elife* **5**, e20390 (2016).
93. Wang, H. et al. Tunicamycin-induced unfolded protein response in the developing mouse brain. *Toxicol. Appl. Pharmacol.* **283**, 157–167 (2015).
94. Abdullahi, A., Stanojic, M., Parousis, A., Patsouris, D. & Jeschke, M. G. Modeling acute ER stress in vivo and in vitro. *Shock* **47**, 506 (2017).
95. Wang, Y.-W. et al. Mild endoplasmic reticulum stress ameliorates lipopolysaccharide-induced neuroinflammation and cognitive impairment via regulation of microglial polarization. *J. Neuroinflamm.* **14**, 1–18 (2017).
96. Stern, A. L. et al. BACE1 mediates HIV-associated and excitotoxic neuronal damage through an APP-dependent mechanism. *J. Neurosci.* **38**, 4288–4300. <https://doi.org/10.1523/JNEUROSCI.1280-17.2018> (2018).
97. Weischenfeldt, J. & Porse, B. Bone marrow-derived macrophages (BMM): Isolation and applications. *CSH Protoc.* **2008**, pdb.prot5080 (2008).

Author contributions

S.G. performed all experiments and wrote the first draft of the manuscript. N.R.B. performed phagocytosis experiments. X.S. performed kinase assays. X.S. and E.A-P. performed animal cohort studies. S.E.B.N. designed the cell-free kinase assay and provided intellectual feedback. C.A-E. designed the kinase assay, provided intellectual feedback, and edited the manuscript. K.L. J-S obtained funding for the study, provided intellectual feedback, and edited the manuscript.

Funding

The funding was provided by National Institutes of Health (No. MH109382).

Competing interests

The authors declare no competing interests.

Additional information

Supplementary Information The online version contains supplementary material available at <https://doi.org/10.1038/s41598-024-74362-z>.

Correspondence and requests for materials should be addressed to K.L.J.-S.

Reprints and permissions information is available at www.nature.com/reprints.

Publisher's note Springer Nature remains neutral with regard to jurisdictional claims in published maps and institutional affiliations.

Open Access This article is licensed under a Creative Commons Attribution-NonCommercial-NoDerivatives 4.0 International License, which permits any non-commercial use, sharing, distribution and reproduction in any medium or format, as long as you give appropriate credit to the original author(s) and the source, provide a link to the Creative Commons licence, and indicate if you modified the licensed material. You do not have permission under this licence to share adapted material derived from this article or parts of it. The images or other third party material in this article are included in the article's Creative Commons licence, unless indicated otherwise in a credit line to the material. If material is not included in the article's Creative Commons licence and your intended use is not permitted by statutory regulation or exceeds the permitted use, you will need to obtain permission directly from the copyright holder. To view a copy of this licence, visit <http://creativecommons.org/licenses/by-nc-nd/4.0/>.

© The Author(s) 2024